

Article

Selective Oxidation of Glycerol via Acceptorless Dehydrogenation Driven by Ir(I)-NHC Catalysts

M. Victoria Jiménez *, Ana I. Ojeda-Amador, Raquel Puerta-Oteo, Joaquín Martínez-Sal, Vincenzo Passarelli  and Jesús J. Pérez-Torrente * 

Departamento de Química Inorgánica, Instituto de Síntesis Química y Catálisis Homogénea-ISQCH, Universidad de Zaragoza-C.S.I.C., 50009 Zaragoza, Spain

* Correspondence: vjimenez@unizar.es (M.V.J.); perez@unizar.es (J.J.P.-T.)

Abstract: Iridium(I) compounds featuring bridge-functionalized bis-NHC ligands (NHC = N-heterocyclic carbene), [Ir(cod)(bis-NHC)] and [Ir(CO)₂(bis-NHC)], have been prepared from the appropriate carboxylate- or hydroxy-functionalized bis-imidazolium salts. The related complexes [Ir(cod)(NHC)₂]⁺ and [IrCl(cod)(NHC)(cod)] have been synthesized from a 3-hydroxypropyl functionalized imidazolium salt. These complexes have been shown to be robust catalysts in the oxidative dehydrogenation of glycerol to lactate (LA) with dihydrogen release. High activity and selectivity to LA were achieved in an open system under low catalyst loadings using KOH as a base. The hydroxy-functionalized bis-NHC catalysts are much more active than both the carboxylate-functionalized ones and the unbridged bis-NHC iridium(I) catalyst with hydroxyalkyl-functionalized NHC ligands. In general, carbonyl complexes are more active than the related 1,5-cyclooctadiene ones. The catalyst [Ir(CO)₂{(MeImCH₂)₂CHOH}]Br exhibits the highest productivity affording TONs to LA up to 15,000 at very low catalyst loadings.

Keywords: glycerol; lactic acid; dehydrogenation; hydrogen release; N-heterocyclic carbenes; iridium; homogeneous catalysis



Citation: Jiménez, M.V.; Ojeda-Amador, A.I.; Puerta-Oteo, R.; Martínez-Sal, J.; Passarelli, V.; Pérez-Torrente, J.J. Selective Oxidation of Glycerol via Acceptorless Dehydrogenation Driven by Ir(I)-NHC Catalysts. *Molecules* **2022**, *27*, 7666. <https://doi.org/10.3390/molecules27227666>

Academic Editor: Angelo Nacci

Received: 24 October 2022

Accepted: 5 November 2022

Published: 8 November 2022

Publisher's Note: MDPI stays neutral with regard to jurisdictional claims in published maps and institutional affiliations.



Copyright: © 2022 by the authors. Licensee MDPI, Basel, Switzerland. This article is an open access article distributed under the terms and conditions of the Creative Commons Attribution (CC BY) license (<https://creativecommons.org/licenses/by/4.0/>).

1. Introduction

Currently, the mainstream of commodities is produced from non-renewable fossil fuel resources. However, the non-sustainable nature of fossil resources demands the development of cleaner methodologies to produce chemicals from alternative resources [1]. In this regard, the use of biomass in the biodiesel industry has led to a vast worldwide production of glycerol that is available on a large scale. In fact, the main byproduct in biodiesel processing is the large quantities of crude glycerol, which represent approximately 10 wt% of the total biodiesel [2]. Lactic acid (LA) is widely used in the food, cosmetics, pharmaceuticals, polymers and fine chemicals industries [3]. The increasing demand for this chemical platform and the disadvantages of the current production of LA from sugar fermentation call for the development of novel methodologies [4]. Therefore, new approaches for the valorization of biomass waste products into value-added chemicals are highly desirable. To date, an attractive method is the catalytic oxidation of glycerol to produce lactic acid (LA) and dihydrogen [5]. In this regard, the search for efficient and selective catalysts should have a favorable impact on the development of this methodology.

Heterogeneous catalysts have already proven successful in the dehydrogenation of glycerol to LA. However, this methodology presents some weaknesses as harsh reaction conditions and low selectivities [6–8]. Recently, homogeneous catalysts based on Ir, Ru or Fe for the conversion of glycerol to LA under mild conditions have been developed [9–11]. In this regard, transition metal catalysts based on PNP pincer ligands have shown remarkable activity in the dehydrogenation of a range of substrates, such as formic acid [12], primary and secondary alcohols [13], including methanol [14,15], nitrogen-containing heterocycles [16] or even oxidative dehydrogenation of glycerol to lactate [17,18].

Currently, Ir-NHCs complexes play a prominent role in the area, as they have been revealed as robust catalysts for a number of dehydrogenation reactions, including the selective oxidation of glycerol [19]. In particular, carbonyl Ir-NHC catalysts such as $[\text{Ir}(\text{CO})_2(\text{Ime})_2]^+$ (Ime = 1,3-dimethylimidazol-2-ylidene) [20], $[\text{Ir}(\text{CO})_2\{\text{MeIm}(\text{pyridin-2-ylmethyl})\}]^+$ [21] or even a related water-soluble zwitterionic iridium catalyst featuring NHC ligands with sulfonate-functionalized wingtips [22,23] have shown an excellent catalytic performance in the selective acceptorless dehydrogenation of glycerol to lactate. Furthermore, it has been shown that bis-NHC ligands provide additional stability to the organometallic complexes due to the chelate coordination mode that makes them more resistant to harsh reaction conditions [24]. In fact, recently, mono- and bimetallic iridium complexes supported by triscarbene ligands were applied to the dehydrogenation of biomass-derived glycerol affording hydrogen and lactate with outstanding turnover frequencies [25]. In addition, the coordination polymer derived from a rigid bis-benzimidazolium precursor featuring $\text{Ir}(\text{CO})_2$ metal fragments assembled via a self-supported strategy allows its recycling more than 30 times without any loss of activity [26]. The excellent catalytic performance exhibited by the bimetallic catalytic system [25], the coordination polymer [26] and the NHC-pyridine iridium catalyst [21] is likely a consequence of the effective suppression of inactive binuclear iridium species formed under the catalytic reaction conditions.

In this context, we envisaged the potential of bridge-functionalized bis-NHC ligands containing potentially hemilabile carboxylate or hydroxyl groups as more stable metal-ligand platforms with improved solubility in polar media. Therefore, the present work focuses on the synthesis of a series of bridge-functionalized bis-NHC iridium(I) complexes with the goal of assessing their catalytic performance for the acceptorless dehydrogenation of glycerol to lactic acid. With this aim, we have selected the bis-imidazolium salts **A** and **B**, precursors of the linker-functionalized bis-NHC ligands 1,1-bis(*N*-methylimidazol-ylidene)-acetate and 1,1'-(2-hydroxy-1,3-propanediyl)bis [3-methyl-imidazol-ylidene), respectively. Imidazolium salt **A** [27] has provided access to a stable metal-ligand platform for the design of rhodium and iridium complexes with application in a range of catalytic transformations [28–31], whereas imidazolium salt **B** has been successfully applied for the preparation of palladium, copper, silver and gold complexes with catalytic applications [32–34]. In addition, related iridium(I) complexes derived from the bridge unfunctionalized bis-imidazolium salt, 1,1'-methylene-bis(3-methylimidazolium) (**C**) [35], and 1-(3-hydroxypropyl)-3-methyl-imidazolium (**D**) [36,37] have also been prepared for comparative purposes (Chart 1).

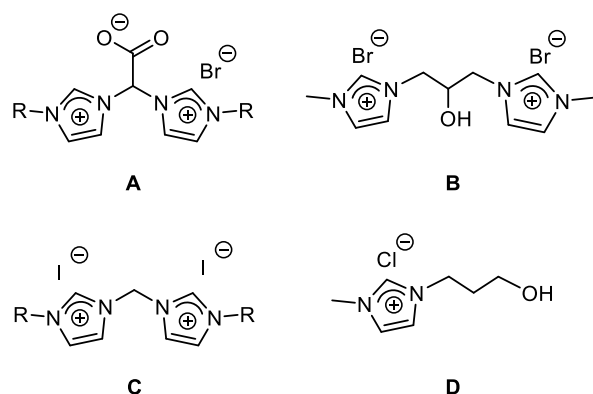


Chart 1. Imidazolium salts precursors of the NHC ligands.

2. Results and Discussion

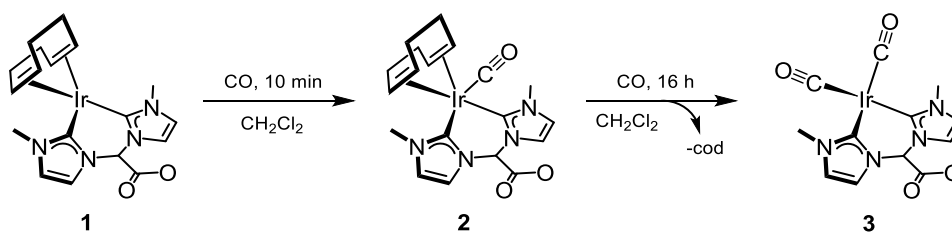
2.1. Synthesis and Characterization of bis-NHC Iridium(I) Complexes

A series of mononuclear bis-NHC iridium(I) catalysts have been synthesized by reaction of the carboxylate- and hydroxy-functionalized bis-imidazolium salts, **A** and **B**, respectively, with appropriate iridium-diene precursors. In addition, a related iridium(I) compound with the unfunctionalized bis-imidazolium salt **C** has also been prepared

(Chart 1). Interestingly, a number of carbonyl rhodium and iridium complexes have found application in several catalytic and thus, related carbonyl bis-NHC iridium(I) have also been prepared by carbonylation of the diene precursors.

2.1.1. Carbonylation of $[\text{Ir}(\text{cod})\{(\text{MeIm})_2\text{CHCOO}\}]$

We have recently reported the synthesis of the zwitterionic iridium(I) $[\text{Ir}(\text{cod})\{(\text{MeIm})_2\text{CHCOO}\}]$ (**1**) (cod = 1,5-cyclooctadiene; MeIm = 3-methylimidazol-2-yliden-1-yl) as a catalyst precursor for the hydrogenation of CO_2 to formate in water [30]. The synthesis of **1** was accomplished by in situ deprotonation of **A** upon reaction with $[\text{Ir}(\mu\text{-OMe})(\text{cod})]_2$ and NaH in MeOH. Bubbling of carbon monoxide through a red suspension of **1** in CH_2Cl_2 for 10 min at room temperature afforded a pale yellow solution from which the five-coordinated iridium(I) complex $[\text{Ir}(\text{CO})(\text{cod})\{(\text{MeIm})_2\text{CHCOO}\}]$ (**2**) was isolated in 78% yield (Scheme 1). The spectroscopic data for **2** agree with the solid-state structure determined by X-ray diffraction methods (see below). The ^1H NMR spectra of **2** showed a set of characteristic resonances indicative of the presence of a coordinated cod ligand. The single absorption band at 1944 cm^{-1} in the ATR-IR spectrum was assigned to the carbonyl ligand, which was observed as a singlet at $\delta 179.0\text{ ppm}$ in the $^{13}\text{C}\{^1\text{H}\}$ NMR spectrum. Furthermore, the ESI+ spectra showed a peak at $m/z 541.1$ with the right isotopic distribution corresponding to the protonated molecular ion. Interestingly, the =CH protons of the cod ligand showed a broad resonance at $\delta 3.90\text{ ppm}$ in the ^1H NMR and a singlet at 71.3 ppm in the $^{13}\text{C}\{^1\text{H}\}$ NMR spectrum, which suggests a dynamic behavior in solution typical of pentacoordinated complexes [38].



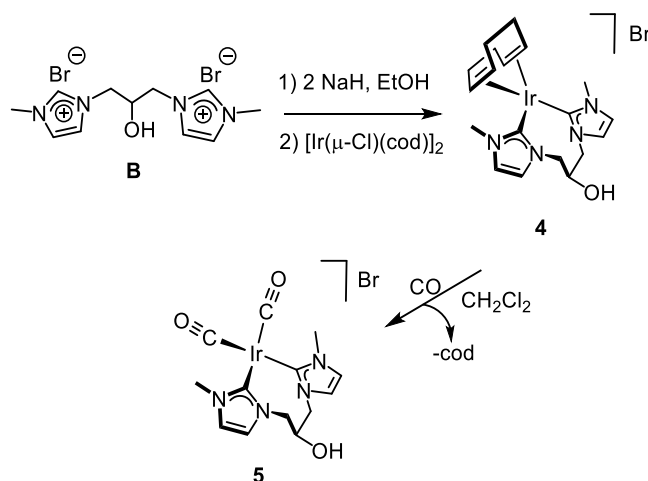
Scheme 1. Synthesis of bis-NHC carbonyl iridium(I) compounds **2** and **3**.

Carbonylation of **1** for longer reaction times easily produces the substitution of the diene ligand to afford the square-planar complex $[\text{Ir}(\text{CO})_2\{(\text{MeIm})_2\text{CHCOO}\}]$ (**3**). Thus, stirring of a red suspension of **1** in CH_2Cl_2 under a carbon monoxide atmosphere for 16 h gave a yellow solution from which **3** was isolated as a yellow solid in 55% yield. This result suggests that the five-coordinated compound **2** is an intermediate in the formation of the square planar carbonyl complex **3** by carbonylation of **1** (Scheme 1). The ESI+ spectra of **3** showed a peak at $m/z 541.1$ with the right isotopic distribution corresponding to the protonated molecular ion. In addition, the ATR-IR spectrum showed two strong carbonyl $\nu(\text{CO})$ bands at 2067 and 2007 cm^{-1} , in accordance with a *cis* dicarbonyl complex. In contrast to the parent diene complex **1**, the ^1H NMR of **3** in CD_3OD showed the presence of a single isomer. In addition, the CHCOO resonance was found rather downfield shifted, around $\delta 6.7\text{ ppm}$, which could be a consequence of the presence of stronger π -acceptor ligands in the coordination sphere of the metal center. On the other hand, the equivalent carbonyl ligands were observed as a singlet at $\delta 183.2\text{ ppm}$ in the $^{13}\text{C}\{^1\text{H}\}$ NMR spectrum.

2.1.2. Synthesis and Reactivity of $[\text{Ir}(\text{cod})\{(\text{MeImCH}_2)_2\text{CHOH}\}]\text{Br}$

To study the possible influence on the catalytic activity of the bridge-chain length, a related hydroxy-functionalized bis-NHC ligand with three carbon atoms in the bridge between both imidazole-2-carbene moieties was selected. The hydroxy-functionalized bis-imidazolium salts $[\{(\text{RImH})\text{CH}_2\}_2\text{CHOH}]\text{Br}_2$ (R = Me, ^iPr , Bn) and their rhodium(I) complexes were synthesized by Herrmann et al. [39]. We have prepared the related iridium(I) compound $[\text{Ir}(\text{cod})\{(\text{MeImCH}_2)_2\text{CHOH}\}]\text{Br}$ (**4**) following a two-steps procedure similar to that described for the synthesis of rhodium(I) complexes and related

unbridged bis-NHC iridium(I) compounds synthesized by us [40] (Scheme 2). First, a solution of the ethoxo-bridge iridium dimer $[\text{Ir}(\mu\text{-OEt})(\text{cod})]_2$ was prepared by reaction of $[\text{Ir}(\mu\text{-Cl})(\text{cod})]_2$ with an excess of NaH in ethanol. Then, the solution was added to a solution of $[\{(\text{MeImH})\text{CH}_2\}_2\text{CHOH}]\text{Br}_2$ in ethanol to give an orange solution from which **4** was isolated as a microcrystalline shiny orange solid in 80% yield. In this synthetic methodology, the bridging ethoxo groups in the iridium dimer are responsible for the deprotonation of one imidazolium moiety, whereas the deprotonation of the second one takes place due to the excess of NaOEt in the reaction medium.



Scheme 2. Synthesis of bis-NHC iridium(I) compounds **4** and **5**.

The ESI+ mass spectra of **4** showed a peak at m/z 521.0, corresponding to the molecular ion with the right isotopic pattern. However, in contrast to the rhodium complex, which exists as a single isomer in solution [39], the ^1H NMR spectrum of **4** in CD_3OD or CD_2Cl_2 showed duplicate signals for all proton resonances, confirming the presence of two isomers. As can be seen in the ^1H NMR spectrum in CD_2Cl_2 at room temperature, both isomers are in a 2/1 ratio (Figure 1). The imidazole-2-carbene ring protons appeared as two sets of doublets at δ 7.37 and 6.80 ppm ($J_{\text{H-H}} = 1.9$ Hz) for the major isomer and at 7.23 and 6.88 ppm ($J_{\text{H-H}} = 1.9$ Hz) for the minor isomer, whereas a broad singlet at δ 6.25 ppm was observed for the hydroxy proton of both isomers. The equivalent N-Me protons of both isomers were observed as two singlets at δ 3.81 ppm for the minor isomer and 3.80 ppm for the major isomer. Two broad signals at δ 4.14 and 4.09 ppm include the =CH olefin protons of both isomers, whereas the $>\text{CH}_2$ protons appeared as a set of broad resonances in the range 2.43–1.95 ppm. Nevertheless, the olefin resonances for the cod ligand were observed as two sets of two singlets at δ 77.2, 76.0 ppm (major isomer) and 77.9, 76.2 ppm (minor isomer) in the $^{13}\text{C}\{^1\text{H}\}$ NMR spectrum, which agrees with the presence of a symmetry plane in each one of the isomers.

Most likely, both isomers result from the different disposition of the hydroxy substituent on the eight-membered metallacycle with a boat-chair conformation, namely pseudo-axial and pseudo-equatorial positions. The major isomer should correspond to the one having the hydroxy group in the pseudo-axial position, similar to the solid-state structure (see below). Interestingly, both isomers can be easily interconverted by inversion of the metallacycle followed by twisting. However, the ^1H - ^1H -NOESY spectrum shows no exchange cross-peaks between the main resonances of both isomers, pointing to a high-energy barrier process, and consequently, both isomers do not interconvert in solution. Finally, it is worth mentioning that the substituent in axial position at carbon-5 in a hypothetical boat-boat conformation of the eight-membered metallacycle remains close to the metal center enabling for anagostic interactions, which is not possible in the boat-chair conformation [41].

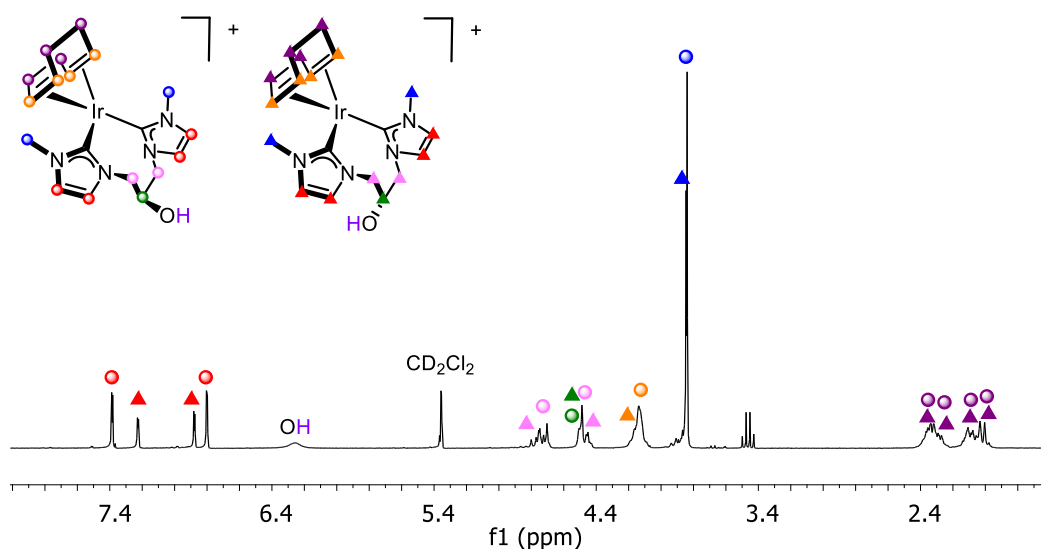


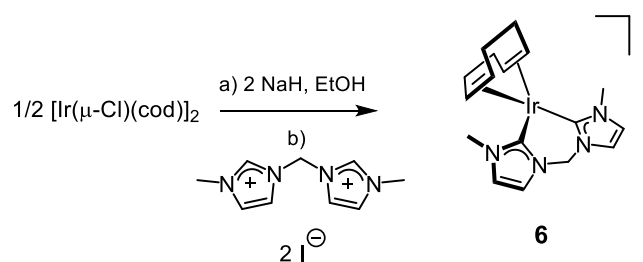
Figure 1. ^1H NMR (CD_2Cl_2 , 298K) spectrum of $[\text{Ir}(\text{cod})\{(\text{MeImCH}_2)_2\text{CHOH}\}]\text{Br}$ (**4**) showing the presence of two isomers.

Carbonylation of $[\text{Ir}(\text{cod})\{(\text{MeImCH}_2)_2\text{CHOH}\}]\text{Br}$ (**4**) in CH_2Cl_2 for 10 min gave a yellow solution of the carbonyl complex $[\text{Ir}(\text{CO})_2\{(\text{MeImCH}_2)_2\text{CHOH}\}]\text{Br}$ (**5**) which was isolated as a microcrystalline yellow solid in 80% yield (Scheme 2). The ESI+ mass spectra of **5** showed a peak at m/z 469.0 with the right isotopic distribution for the molecular ion. In addition, the ATR-IR spectrum displayed two strong absorption bands at 2058 and 1985 cm^{-1} suggesting the existence of two metal-bounded carbonyl ligands in *cis* disposition. As shown by the ^1H NMR spectrum, solutions of complex **5** in CD_2Cl_2 contain two isomers in a 4/1 ratio (see the Supporting Information). The imidazole-2-carbene ring protons appeared as two doublets for each isomer in the range δ 7.54–6.93 ppm ($J_{\text{H-H}} = 1.9\text{ Hz}$), whereas the linker $>\text{CH}_2$ protons appeared as a set of complex resonances in the range 4.69–4.41 ppm. The equivalent carbonyl ligands of both isomers of **5** were observed as a singlet at δ 182.3 ppm in the $^{13}\text{C}\{^1\text{H}\}$ -apt spectrum. Although duplicate signals for each carbon resonance were observed in the spectrum, a single resonance at δ 169.3 ppm, highfield shifted compared to that of the parent complex **4**, was observed for both isomers.

As described for complex **4**, the two isomers likely arise from the different disposition of the hydroxy substituent in pseudo-axial and pseudo-equatorial positions in the eight-membered metallacycle adopting a boat-chair conformation, with the major isomer having the hydroxy group in pseudo-axial position (see below). As in the case of **4**, the ^1H - ^1H -NOESY spectrum evidences that both isomers are not interconverting in solution. Although the isomer ratio found in both compounds, 2/1 for **4** and 4/1 for **5**, could be a consequence of the different solubility, an isomerization along the carbonylation process cannot be excluded.

2.1.3. Synthesis of $[\text{Ir}(\text{cod})\{(\text{MeIm})_2\text{CH}_2\}]\text{I}$

The cationic complex $[\text{Ir}(\text{cod})\{(\text{MeIm})_2\text{CH}_2\}]\text{I}$ (**6**) has been prepared following the two-step procedure described by Herrmann et al. for the rhodium complex $[\text{Rh}(\text{cod})\{(\text{MeIm})_2\text{CH}_2\}]\text{I}$ [42,43]. To the best of our knowledge, the iridium complex **6** has not been reported yet. The reaction of the unfunctionalized bis-imidazolium salt $[(\text{MeIm})_2\text{CH}_2]\text{I}_2$ (**C**) with the ethoxo-bridged iridium dimer $[\text{Ir}(\mu\text{-OEt})(\text{cod})]_2$, prepared in situ by reaction of $[\text{Ir}(\mu\text{-Cl})(\text{cod})]_2$ with an excess of NaH in ethanol, in the presence of the excess of NaOEt afforded complex **6** as an orange solid in 63% yield (Scheme 3). The ^1H NMR of **6** in CD_2Cl_2 showed two doublets at δ 6.03 and 5.82 ppm ($J_{\text{H-H}} = 11.9\text{ Hz}$) for the diastereotopic protons of the bridging methylene protons and a broad multiplet at 3.82 ppm for the $=\text{CH}$ protons of the cod ligand which agrees with the proposed square planar structure.



Scheme 3. Synthesis of the bis-NHC iridium(I) compound **6**.

2.1.4. Crystal and Molecular Structure of bis-NHC Iridium(I) Compounds

The crystal structure of $[\text{Ir}(\text{CO})(\text{cod})\{(\text{MeIm})_2\text{CHCOO}\}]\cdot 2\text{CH}_3\text{OH}$ ($2\cdot 2\text{CH}_3\text{OH}$) exhibits an asymmetric unit with two crystallographically independent complexes along with four CH_3OH molecules. Despite the fact that one of the two metal complexes contains a partially disordered cod ligand, the two metal complexes of the asymmetric unit are chemically equivalent and virtually superimposable. On this ground, only the molecular structures of one of them will be discussed herein in detail. The ORTEP view of the solid-state structures of $2\cdot 2\text{CH}_3\text{OH}$ is shown in Figure 2a, and selected bond lengths and angles are given in Table 1. A distorted trigonal bipyramidal coordination of the metal center is observed at the metal center, with the carbon monoxide ligand in the equatorial plane. Both the bis-NHC ligand, $(\text{MeIm})_2\text{CHCOO}^-$, and cod ligands are bidentate, each occupying an equatorial coordination site and an axial one, the bite angles of cod $[\text{CT}1-\text{Ir}-\text{CT}2\ 83.559(8)^\circ]$ and $(\text{MeIm})_2\text{CHCOO}^-$ $[\text{C}(1)-\text{Ir}(1)-\text{C}(9)\ 83.6(2)^\circ]$ nicely fitting in with the observed coordination geometry. As for $(\text{MeIm})_2\text{CHCOO}^-$, the bidentate coordination renders a six-membered $\text{Ir}1-\text{C}1-\text{N}5-\text{C}7-\text{N}8-\text{C}9$ metallacycle exhibiting a boat conformation, with Ir1 and C7 occupying out-of-plane positions (interplane angles: 34.3° , C7; 26.0° , Ir), with the equatorial $\text{Ir}1-\text{C}9$ bond length $[2.089(6)\ \text{\AA}]$ slightly longer than the axial $\text{Ir}1-\text{C}1$ $[2.023(6)\ \text{\AA}]$. On the other hand, when dealing with the coordinated olefin groups of cod, the axial $\text{Ir}-\text{CT}1$ distance $[\text{Ir}1-\text{CT}1\ 2.1679(2)\ \text{\AA}]$ is significantly longer than the equatorial $\text{Ir}-\text{CT}2$ one $[\text{Ir}1-\text{CT}2\ 2.0183(2)\ \text{\AA}]$, reasonably as a consequence of the trans influence of the NHC occupying the axial position trans to C17–C18. Accordingly, the C17–C18 bond length $[1.373(8)\ \text{\AA}]$ is shorter than the C21–C22 one $[1.446(8)\ \text{\AA}]$ suggesting a higher metal-ligand back-donation in the case of C21–C22. When dealing with peripheral carboxylato group, similar to what previously observed in related rhodium(I) [27] and iridium(I) [30] $[\text{M}(\text{diene})\{(\text{MeIm})_2\text{CHCOO}\}]$ complexes (diene = cod, nbd), the carboxylate group occupies the flagpole position and the carbon-oxygen bond lengths are similar, indicating that the formal negative charge is delocalized. In addition, both oxygen atoms are involved in an $\text{O}\cdots\text{HO}$ hydrogen bond with lattice methanol (Figure 2a).

Tiny single crystals of $4\cdot 1.75\text{CH}_2\text{Cl}_2$ were grown by slow diffusion of diethyl ether in a solution of **4** in dichloromethane. Weak diffraction patterns were observed (see Experimental Section), and, as a consequence, the quality of the collected data is poor, and the accuracy of the resulting structural determination is low. Nonetheless, the quality of the refined model is good enough to confirm the molecular structure proposed for **4** and will be discussed herein. The asymmetric unit contains two crystallographically independent cations $[\text{Ir}(\text{cod})\{(\text{MeImCH}_2)_2\text{CHOH}\}]^+$ along with two bromide ions and 3.5 molecules of CH_2Cl_2 . Since the independent cations $[\text{Ir}(\text{cod})\{(\text{MeImCH}_2)_2\text{CHOH}\}]^+$ are chemically equivalent, and their structures are virtually superimposable, for the sake of brevity, only one of them will be discussed in the following (Figure 2b). A square planar geometry at the metal center is observed with the bis-NHC ligand occupying two mutually cis positions $[\text{C}(1)-\text{Ir}(1)\ 2.025(13)\ \text{\AA}$, $\text{C}(11)-\text{Ir}(1)\ 2.011(12)\ \text{\AA}$, $\text{C}(11)-\text{Ir}(1)-\text{C}(1)\ 84.1(5)^\circ]$ rendering an eight-membered metallacycle that exhibits a boat-chair conformation with the hydroxy group in the pseudo-axial position. Coordinated cod also acts as a bidentate chelating ligand $[\text{CT}01-\text{Ir}1-\text{CT}02\ 86.476(18)^\circ]$ completing the coordination sphere of the metal center. As for the coordinated olefinic moieties, similar carbon-carbon bond

lengths [C(17)–C(18) 1.352(19) Å, C(21)–C(22) 1.391(18) Å] and similar metal-centroid distances are observed [Ir1–CT01 2.0378(5) Å, Ir1–CT02 2.0708(5) Å]. Interestingly, an OH...Br hydrogen bond was observed between the peripheral group O16–H16 of the bis-NHC ligand and the bromide counterion Br1 (Figure 2b). In addition, the NHC cores lie almost perpendicular to the coordination plane (*av.* 83°), and their pitch and yaw angles (see Experimental Section) indicate a distorted arrangement with respect to the corresponding metal-carbon bond. For the sake of comparison, the structure of the related rhodium complex [Rh(cod){(EtImCH₂)₂CHOH}]⁺ [39] is similar to that described herein for 4.

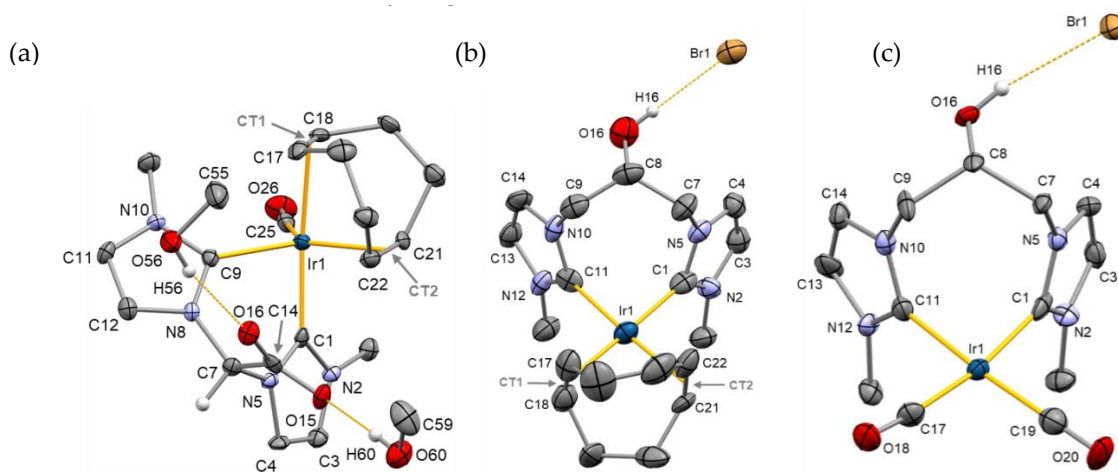


Figure 2. ORTEP plot of 2 in 2:2 CH₃OH (a), 4 in 4:1.75 CH₂Cl₂ (b), and 5 in 5:CH₂Cl₂ (c). Thermal ellipsoids are at 50% of probability. For clarity, most hydrogen atoms are omitted. CT, the centroid of olefinic carbons. Hydrogen bond parameters (Å, deg): 2: O(56)–H(56)···O(16): O(56)–H(56) 0.84, H(56)···O(16) 1.90, O(56)···O(16) 2.714(6), O(56)–H(56)–O(16) 162.4; O(60)–H(60)···O(15): O(60)–H(60) 0.84, H(60)···O(15) 1.87, O(60)···O(15) 2.714(6) O(60)–H(60)···O(15) 176.3. 4: O(16)–H(16)···Br(1): O(16)–H(16) 0.84 H(16)···Br(1) 2.36 O(16)···Br(1) 3.189(9), O(16)–H(16)–Br(1)170.6. 5: O(16)–H(16)···Br(1): O(16)–H(16) 0.84, H(16)···Br(1) 2.42, O(16)···Br(1) 3.252(9) O(16)–H(16)–Br(1) 169.5.

The crystal structure of 5·CH₂Cl₂ contains two crystallographically independent complexes along with two CH₂Cl₂ molecules. Since the two cations are chemically equivalent and virtually superimposable, only one of them will be discussed in detail. A distorted square planar coordination geometry is observed (Figure 2c) with the bis-NHC ligand occupying two mutually cis positions [C(1)–Ir(1) 2.056(14) Å, C(11)–Ir(1) 2.083(13) Å, C(1)–Ir(1)–C(11) 80.4(5)°]. Two carbon monoxide ligands complete the coordination sphere [C(17)–Ir(1)–C(1) 171.1(5)°, C(19)–Ir(1)–C(11) 174.0(6)°], similar metal-carbon [C(17)–Ir(1) 1.876(14) Å, C(19)–Ir(1) 1.883(15)°] and carbon-oxygen bond lengths being observed [C(17)–O(18) 1.131(16) Å, C(19)–O(20) 1.151(17)°]. As observed for 4, the eight-membered metallacycle in 5 adopts a boat-chair conformation with the hydroxy group in the pseudo-axial position. In addition, OH...Br hydrogen bonds are observed between the peripheral O16–H16 group of the bis-NHC ligand and bromide (Figure 2c). Both NHC cores lie almost perpendicular to the coordination plane (81.6, 84.5°), and their pitch and yaw angles indicate that they deviate from the ideal coordination to the metal center, which is reasonably a consequence of crystal packing.

Table 1. Selected bond lengths (Å) and angles (°) in 2·2 CH₃OH, 4·1.75 CH₂Cl₂, and 5·CH₂Cl₂.

	2	4	5
Ir–C(1)	2.023(6)	2.025(13)	2.056(14)
C(9)–Ir(1)	2.089(6)	-	-
C(25)–Ir(1)	1.929(6)	-	-
C(25)–O(26)	1.139(7)	-	-
Ir–C(11)	-	2.011(12)	2.083(13)
Ir–C(17)	-	-	1.876(14)
Ir–C(19)	-	-	1.883(15)
Ir1–CT01	2.1679(2)	2.0378(5)	-
Ir1–CT02	2.0183(2)	2.0708(5)	-
C(17)–C(18)	1.373(8)	1.352(19)	-
C(21)–C(22)	1.446(8)	1.391(18)	-
C(14)–O(16)	1.239(7)	-	-
C(14)–O(15)	1.245(7)	-	-
C(17)–O(18)	-	-	1.131(16)
C(19)–O(20)	-	-	1.151(17)
C(1)–Ir(1)–C(11)	-	84.1(5)	80.4(5)
C(1)–Ir(1)–C(9)	83.6(2)	-	-
CT01–Ir1–CT02	83.559(8)	86.476(18)	-
C1–Ir1–CT01	171.44(15)	-	-
C25–Ir1–CT02	128.21(17)	-	-
CT02–Ir1–C9	129.68(15)	-	-
C(25)–Ir(1)–C(9)	102.0(2)	-	-
C(17)–Ir(1)–C(19)	-	-	93.6(6)
C(17)–Ir(1)–C(1)	-	-	171.1(5)
C(19)–Ir(1)–C(11)	-	-	174.0(6)

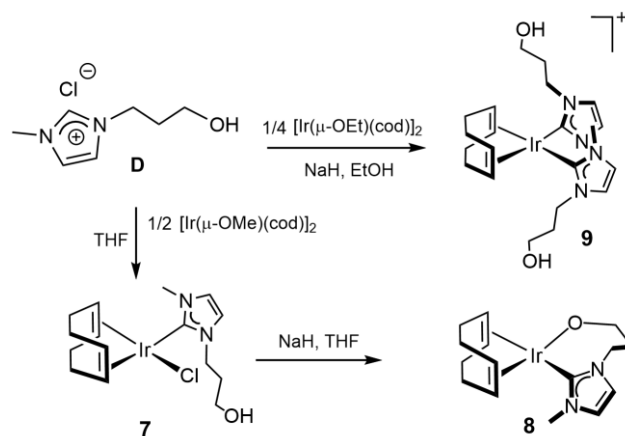
2.2. Synthesis and Characterization of NHC Iridium(I) Complexes

The synthesis of a cationic unbridged bis-NHC iridium(I) complex bearing 3-hydroxypropyl functionalized NHC ligands has been carried out to evaluate the flexibility imparted by two monodentate NHC ligands on the catalytic activity. In addition, neutral complexes having a monodentate NHC ligand have also been prepared for comparative purposes.

Compound [IrCl(cod){MeIm(CH₂)₃OH}] (**7**) was prepared by deprotonation of the functionalized imidazolium salt [MeImH(CH₂)₃OH]Cl (**D**) by the bridging methoxo ligands of compound [[Ir(μ-OMe)(cod)]₂], and isolated as a yellowish solid in 86% yield. The MS spectrum and the conductivity measurements in acetone support the proposed square planar structure featuring a chlorido ligand and an uncoordinated 3-hydroxypropyl wingtip at the NHC ligand. The formation of the Ir–NHC bond was confirmed by the absence of the ¹H signal of the C₂H group of **D** and the presence of a ¹³C{¹H} singlet resonance at δ 180.2 ppm assigned to the carbenic carbon atom. The =CH protons of the cod ligand showed four distinct resonances both the ¹H and ¹³C{¹H} NMR spectra, thereby suggesting restricted rotation about the Ir–CNHC bond. As a consequence, the methylene protons of the 3-hydroxypropyl wingtip are diastereotopic and showed two well-separated resonances in the ¹H NMR spectra. On the other hand, the hydroxyl group has been identified indirectly at δ 3.14 ppm since the signal does not correlate with any carbon in the two-dimensional ¹H, ¹³C-HSQC spectra (see Supporting Information).

The hydroxy group at the wingtip of compound **7** can be easily deprotonated to afford the neutral alkoxo compound [Ir(cod){κ²-C,O-{MeIm(CH₂)₃O}] (**8**) with the functionalized NHC ligand exhibiting a κ²-C,O coordination mode rendering a seven-membered metallacycle. Thus, the reaction of **7** with one equiv of NaH in anhydrous tetrahydrofuran gave, after removal of the formed sodium chloride, an orange solution from which compound **8** was isolated as an orange solid in 82% yield (Scheme 4). The neutral character of **8** was confirmed by conductivity measurements in acetone. In addition, the MALDI-Tof mass spectrum showed a peak at *m/z* 441.29, corresponding to the protonated molecular ion. The ¹H and ¹³C{¹H} NMR spectra are consistent with the unsymmetrical structure resulting

from the conformational constraint imposed by the coordination of the alkoxy fragment to the metal center. It is noticeable the deshielding of the olefinic proton resonance of the 1,5-cyclooctadiene ligand trans to the alkoxy group in the ^1H NMR spectra, from 4.61 and 4.54 ppm in **7** to 5.11 and 5.05 ppm in **8**, which is diagnostic for the coordination of the alkoxy group to the metal center [44].



Scheme 4. Synthesis of NHC iridium(I) compounds 7–9.

The unbridged bis-carbene compound $[\text{Ir}(\text{cod})\{\text{MeIm}(\text{CH}_2)_3\text{OH}\}_2]\text{Cl}$ (**9**) has been synthesized via deprotonation of the imidazolium salt **D** by the bridging ethoxo ligands in the dimer $[\text{Ir}(\mu\text{-OEt})(\text{cod})]_2$, generated in situ by reaction of $[\text{Ir}(\mu\text{-Cl})(\text{cod})]_2$ with NaH in ethanol, in the presence of an excess of NaOEt (Scheme 4). The complex was obtained as an orange-yellow microcrystalline solid with a 72% yield after the removal of the inorganic salts.

The cationic character of the compound was established by conductivity measurements. However, the molar conductivity value, $55 \Omega^{-1} \text{cm}^2 \text{mol}^{-1}$, is appreciably below that expected for 1:1 electrolytes in acetone, which is attributed to the formation of ionic pairs due to the presence of polar wingtips at the NHC ligands. In addition, the mass spectra (ESI⁺, MeOH) showed the molecular ion with the right isotopic pattern at m/z 581.2468. The ^1H NMR of **9** exhibited duplicated resonances for both cod and NHC ligands, which evidenced the presence of two symmetrical isomers. For example, the =CH protons of the imidazole-2-ylidene rings showed two sets of resonances in a 70/30 ratio, and two low field resonances at δ 177.8 and 176.6 ppm for the carbene carbon atoms of both isomers were observed in the $^{13}\text{C}\{^1\text{H}\}$ NMR. The presence of two diastereomers for **9** is derived from the relative disposition of the 3-hydroxypropyl functionalized NHC ligands: the *up-down* isomer (C_2 symmetry) and the *up-up* isomer (C_s symmetry) having antiparallel and parallel arrangement of the carbene ligands, respectively (Figure 3). It should be noted that related compounds $[\text{Ir}(\text{cod})(\text{NHC}\text{rZ})_2]^+$ (rZ = 2-methoxybenzyl; pyridin-2-ylmethyl and quinolin-8-ylmethyl) also exist as two diastereomers that interconvert in solution in which the “up-down” is the major diastereomer [40].

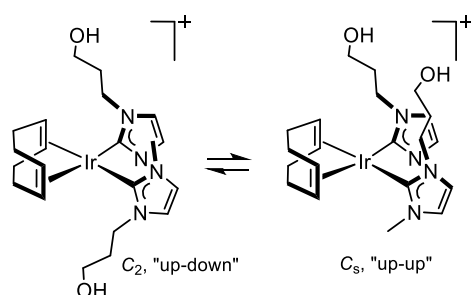


Figure 3. Equilibrium between the two diastereomers of compound $[\text{Ir}(\text{cod})\{\text{MeIm}(\text{CH}_2)_3\text{OH}\}_2]\text{Cl}$ (**9**).

The assignment of the ^1H and $^{13}\text{C}\{^1\text{H}\}$ resonances of both diastereomers of **9** was achieved by a combination of the $^1\text{H}-^1\text{H}$ COSY, ^{13}C APT, and $^1\text{H}-^{13}\text{C}$ HSQC spectra. Remarkably, the

bidimensional ^1H – ^1H -NOESY spectrum showed strong exchange cross-peaks between all types of protons for both species, together with weak NOE cross-peaks, indicating that both diastereomers interconvert in solution (see the Supporting Information).

2.3. Dehydrogenation of Glycerol to Lactic Acid

The described iridium(I) complexes **1** and **3–9** have been evaluated as catalysts for the acceptorless dehydrogenation of glycerol to produce lactic acid and H_2 . The influence of the functional group in the bridge on the catalytic activity of bis-NHC iridium complexes, as well as that of the auxiliary ligands, has been investigated and compared with that of complexes featuring functionalized monodentate NHC ligands. The reactions were performed in an open flask using neat glycerol and KOH as a base in the presence of the iridium catalyst. The catalytic performance of the catalysts with different base/catalyst ratios at diverse temperatures is summarized in Table 2.

No formation of lactate (LA) or other glycerol derivatives was observed with catalysts **1** and **4** in the absence of a base (entries 1–2) or in the absence of the catalyst (entry 3) after a prolonged reaction time at 115 °C. On the other hand, blank tests with the imidazolium salts A–D (Chart 1) provide no glycerol conversion. Preliminary catalytic tests with the bis-NHC carbonyl complexes **3** and **5** (1 mol%) using KOH as a base in glycerol/water (1:1) under very mild temperature conditions gave good glycerol conversions albeit moderate selectivities for LA, due to the formation of 1,2-propane diol, with turnover numbers for the production of lactate, TON_{LA} , of ca. 200 (entries 4 and 5) which shows the potential of this family of catalysts for acceptorless dehydrogenation of glycerol. In light of these results, the reaction conditions were optimized in order to reduce the catalyst loading and improve the selectivity towards lactate salt. So, to compare the catalytic performance of the iridium(I) catalysts, we have selected the following standard catalytic reaction conditions: 5 mmol of KOH, catalyst loading of 0.2 mol% (relative to the limiting reagent KOH), in neat glycerol at 130 °C.

Under the standard catalytic reaction conditions, all complexes **1** and **3–9** are active for the acceptorless dehydrogenation of neat glycerol (entries 6–13) with good selectivities, in the range 86–100%, for LA. In the cases where selectivity does not reach 100%, the only byproduct detected is 1,2-propanediol. The more active catalysts **4**, **5** and **7** provided conversions higher than 60% in only 2 h with selectivities higher than 85%. Among them, catalyst $[\text{Ir}(\text{CO})_2\{\text{MeImCH}_2\}_2\text{CHOH}]\text{Br}$ (**5**) exhibited the best catalytic performance with an adequate balance of activity and selectivity with a TON_{LA} superior to 400 (entry 9). In general, carbonyl complexes are more active than diene complexes. As for the bis-NHC complexes, bridge-functionalized complexes are more active than compound **6**, featuring an unfunctionalized bis-NHC ligand. In addition, the hydroxy-functionalized bis-NHC complexes **4** and **5**, are much more active than the carboxylate-functionalized complexes **1** and **3**. The excellent catalytic performance of $[\text{IrCl}(\text{cod})\{\text{MeIm}(\text{CH}_2)_3\text{OH}\}]$ (**7**), TON_{LA} of 344, contrast with that of the alkoxo compound **8** and the unbridged bis-NHC compound **9** (entries 11–13).

Other inorganic bases, such as NaOH or Cs_2CO_3 , have also been investigated under standard conditions using catalyst **7**. The catalyst performance was much worse with Cs_2CO_3 , and with NaOH, it took 6 h to achieve the same conversion (entries 14–15). The better performance of KOH is likely related to the higher solubility of potassium hydroxide in glycerol. Increasing the temperature from 130 to 150 °C resulted in an increase in activity, reaching similar conversions in only 0.75 h and selectivities to LA higher than 90% (entries 16–20). Under these conditions, catalyst **5** was the most efficient, with total conversion and a 93% selectivity to LA (entry 19). On the other hand, the influence of the amount of KOH on the catalytic activity has also been studied using the same amount of catalyst **5** (0.01 mmol, entry 19). A decrease in the amount of KOH leads to a drastic decrease in LA formation (entries 21–22), and the activity did not improve when the amount of KOH was increased to 6 mmol (entry 23). Interestingly, it was possible to reduce the catalyst load to 0.07 mol% achieving good conversion in 24 h and full conversion to LA in 72 h. Excellent

selectivity to LA was also attained when the reaction was performed in a glycerol/H₂O (1:1), albeit with moderate conversion (entries 24–26). The catalyst loading can be reduced to 70 ppm (0.007 mol%), attaining 74% conversion in 72 h with complete selectivity to LA. Further reduction of the catalyst loading to 14 ppm (0.0014 mol%) allows a remarkable TON_{LA} of 15,000 (entries 27 and 28).

Table 2. Dehydrogenation of Neat Glycerol to Lactic Acid ^a.

Entry	Catalyst	Base (mmol)	t [h]	T [°C]	Conv. [%] ^b	Select. LA(%) ^b	TON _{LA} ^c
1	1 (1)	-	66	115	0	0	0
2	4 (1)	-	66	115	0	0	0
3	-	KOH (5)	66	115	0	0	0
4	3 (1) ^d	KOH (5)	36	115	67	59	198
5	5 (1) ^d	KOH (5)	36	115	69	76	262
6	1 (0.2)	KOH (5)	2	130	24	93	112
7	3 (0.2)	KOH (5)	2	130	30	98	147
8	4 (0.2)	KOH (5)	2	130	61	93	284
9	5 (0.2)	KOH (5)	2	130	91	92	419
10	6 (0.2)	KOH (5)	2	130	15	100	75
11	7 (0.2)	KOH (5)	2	130	80	86	344
12	8 (0.2)	KOH (5)	2	130	35	98	172
13	9 (0.2)	KOH (5)	2	130	56	92	258
14	7 ^e	NaOH (5)	6	130	78	80	312
15	7 ^e	Cs ₂ CO ₃ (5)	25	130	23	84	97
16	1 (0.2)	KOH (5)	0,75	150	31	93	144
17	3 (0.2)	KOH (5)	0,75	150	40	94	188
18	4 (0.2)	KOH (5)	0,75	150	71	92	327
19	5 (0.2)	KOH (5)	0,75	150	100	93	465
20	7 (0.2)	KOH (5)	0,75	150	70	92	322
21	5 (0.2)	KOH (0.5)	0,75	150	15	59	44
22	5 (0.2)	KOH (2.5)	0,75	150	80	57	228
23	5 (0.2)	KOH (6)	0,75	150	91	91	414
24	5 (0.07)	KOH (5)	24	150	91	71	923
25	5 (0.07) ^d	KOH (5)	24	150	68	100	971
26	5 (0.07)	KOH (5)	72	150	100	70	1000
27	5 (0.007)	KOH (5)	72	150	74	100	10,571
28	5 (0.0014)	KOH (5)	72	150	21	100	15,000

^a Standard reaction conditions: glycerol (1 mL, 13.7 mmol), KOH (5 mmol) and iridium catalyst (mol% relative to the limiting reagent KOH) in an open flask. ^b Conversion of glycerol, based on the theoretical maximum determined by the mmol of the added base, and selectivity for potassium lactate (LA) were determined by ¹H NMR using NaOAc as internal standard. ^c TON_{LA} calculated as the mol of LA produced per mol of catalyst. ^d glycerol (0.5 mL) and H₂O (0.5 mL). ^e 0.01 mmol of catalyst.

The catalytic experiments of Table 2 were performed in an open flask allowing the release of the H₂(g) produced in the dehydrogenation of glycerol. The catalytic dehydrogenation reactions were also performed in a close microreactor equipped with a pressure transducer to monitor the H₂(g) evolution along the catalytic reaction. The reactions were carried out in neat glycerol using KOH as a base (5 mmol) and a catalyst loading of 0.2 mol% of iridium catalysts at 130 °C. In general, the reactions in a closed reactor are slower than in an open system. However, good conversions were obtained after 5 h. The reaction profiles for catalysts [Ir(cod){(MeIm)₂CHCOO}] (1), [Ir(cod){(MeImCH₂)₂CHOH}]Br (4) and [IrCl(cod){MeIm(CH₂)₃OH}] (7) are shown in Figure 4. Catalysts 1 and 7 exhibited a similar behavior which contrasts with the excellent activity of catalyst 4 under these conditions. Nevertheless, the kinetic profiles are quite similar for all of them, showing a very short

induction period for catalyst preactivation. In all three cases, the amount of hydrogen released after 5 h of reaction is below the stoichiometric limit determined by the KOH added (5 mmol), which results in conversions of 94% (**4**), 84% (**1**) and 81% (**7**). The ^1H NMR spectra in D_2O of the resultant reaction mixture for all three catalytic tests showed the presence of the intermediate 1,2-propanediol in ca. 10%, but not degradation products derived from glycerol overoxidation or glycerol C–C cleavage (see Supporting Information).

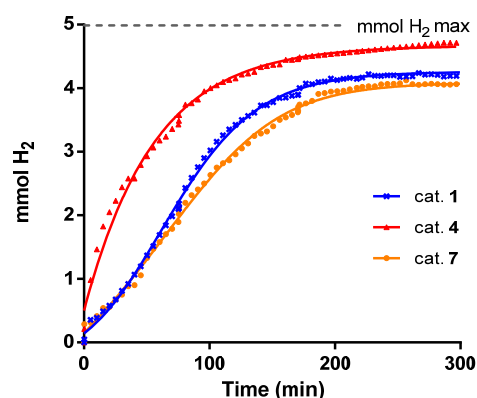
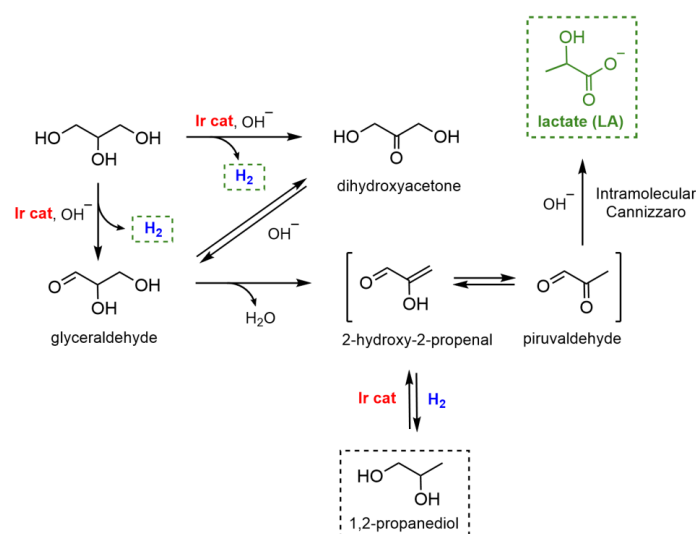


Figure 4. Evolution of $\text{H}_2(\text{g})$ vs. time for the dehydrogenation of glycerol to lactic acid catalyzed by **1**, **4** and **7** (0.2 mol%) at $130\text{ }^\circ\text{C}$. The produced hydrogen in the catalytic tests is consistent with the stoichiometric limit of added KOH (5 mmol of $\text{H}_2(\text{g})$, horizontal line).

These results show that in the presence of molecular hydrogen (closed flask), not only the activity decreases but also the selectivity due to the increases in the amount of propanediol, which is consistent with the commonly accepted mechanism for glycerol dehydrogenation by iridium catalysts [20]. We assumed that glycerol conversion likely proceeds through the acceptorless iridium-catalyzed dehydrogenation of glycerol to dihydroxyacetone or glyceraldehyde, which interconverts in the presence of a base. Subsequent base-catalyzed dehydration of glyceraldehyde would lead to pyruvaldehyde which reacts by an intramolecular Cannizzaro reaction to yield LA. However, the hydrogenation of the enol-pyruvaldehyde tautomer by the iridium catalyst would lead to 1,2-propanediol, which is the main byproduct of the reaction and is favored under hydrogen pressure. Subsequently, the dehydrogenation of 1,2-propanediol, which is inhibited under hydrogen, results in the formation of pyruvaldehyde (Scheme 5).



Scheme 5. Proposed mechanism for the conversion of glycerol to lactate and hydrogen and commonly related byproducts.

3. Experimental Section

3.1. Materials and Methods

Experiments under an atmosphere of argon were carried out using Schlenk techniques or in a dry box. Solvents were distilled immediately prior to use from the appropriate drying agents or obtained from a Solvent Purification System (Innovative Technologies). Oxygen-free solvents were employed throughout. CDCl_3 , CD_2Cl_2 and benzene- d_6 were dried using activated molecular sieves. Methanol- d_4 (<0.02% D_2O) was purchased from Eurisotop and used as received. The imidazolium salts, 1,1-bis(*N*-methylimidazolium)-acetate-bromide, $[(\text{MeImH})_2\text{CHCOO}]\text{Br}$ (**A**) [30], 1,1'-(2-hydroxy-1,3-propanediyl)bis[3-methyl-1*H*-imidazolium]dibromide, $[(\text{MeImHCH}_2)_2\text{CHOH}]\text{Br}_2$ (**B**) [39], 1,1'-methylenebis(3-methylimidazolium)diiodide, $[(\text{MeIm})_2\text{CH}_2]\text{I}_2$ (**C**) [35], and 1-(3-hydroxypropyl)-3-methyl-1*H*-imidazol-3-ium chloride, $[\text{MeImH}(\text{CH}_2)_3\text{OH}]\text{Cl}$ (**D**) [36], were prepared according to the literature. The starting materials $[\text{Ir}(\mu\text{-Cl})(\text{cod})]_2$ [45], and $[\text{Ir}(\mu\text{-OMe})(\text{cod})]_2$ [46], and compound $[\text{Ir}(\text{cod})\{\text{MeIm}\}_2\text{CHCOO}]$ (**1**) [30], were prepared following the procedures previously reported.

3.2. Scientific Equipment

C, H, and N analyses were carried out in a PerkinElmer 2400 Series II CHNS/O analyzer. Infrared spectra were recorded on an FT-PerkinElmer Spectrum One spectrophotometer using Nujol mulls between polyethylene sheets. ^1H NMR spectra were recorded on a Bruker Avance 300 (300.128 MHz and 75.479 MHz) or Bruker Avance 400 (400.130 MHz and 100.613 MHz). NMR chemical shifts are reported in ppm relative to tetramethylsilane and are referenced to partially deuterated solvent resonances. Coupling constants (*J*) are given in hertz. Spectral assignments were achieved by a combination of ^1H – ^1H COSY, ^{13}C APT, ^1H – ^{13}C HSQC and ^1H – ^{13}C HMBC experiments. High-resolution electrospray ionization mass spectra (HRMS-ESI) were recorded using a Bruker MicroToF-Q equipped with an API-ESI source and a Q-ToF mass analyzer, which leads a maximum error in the measurement of 5 ppm, using sodium formate as reference. MALDI-TOF mass spectra were obtained on a Bruker MICROFLEX spectrometer using DIT, ditranol, 1,8-dihydroxy-9,10-dihydroanthracen-9-one, as matrix [47]. Conductivities were measured in ca. 5×10^{-4} M acetone solutions of the complexes using a Philips PW 9501/01 conductimeter.

3.3. Compound Synthesis

3.3.1. Synthesis of $[\text{Ir}(\text{CO})(\text{cod})\{\text{MeIm}\}_2\text{CHCOO}]$ (**2**), Figure 5

Carbon monoxide was bubbled through a solution of $[\text{Ir}(\text{cod})\{\text{MeIm}\}_2\text{CHCOO}]$ (**1**) (25.0 mg, 0.048 mmol) in CH_2Cl_2 (5 mL) for 10 min to give a pale-yellow solution. The concentration of the solution to ca. 1 mL and the slow addition of diethyl ether afforded the compound as a yellow solid that was filtered, washed with cold diethyl ether (3×3 mL) and dried in vacuo. Yield: 18.9 mg, 72%. Anal. Calc. for $\text{C}_{19}\text{H}_{23}\text{IrN}_4\text{O}_3 \cdot \text{CH}_3\text{OH}$: C, 41.44; H, 4.69; N, 9.66. Found: C, 41.56; H, 4.61; N, 9.70. MS (ESI+, $\text{CH}_2\text{Cl}_2/\text{MeOH}$, *m/z*): calcd. for $\text{C}_{19}\text{H}_{24}\text{IrN}_4\text{O}_3$ $[\text{M}+\text{H}]^+$: 549.15, found: 549.10. IR (ATR, cm^{-1}): 1944 (CO), 1635 (COO). ^1H NMR (298 K, 300 MHz, CD_3OD): δ 7.44 (d, *J* = 2.0, 2H, CH), 7.28 (d, *J* = 2.0, 2H, CH), 6.73 (s, 1H, CHCOO), 3.90 (br, 4H, =CH cod), 3.68 (s, 6H, NCH_3), 2.64–2.45 (m, 4H, $>\text{CH}_2$ cod), 2.41–2.21 (m, 4H, $>\text{CH}_2$ cod). $^{13}\text{C}\{^1\text{H}\}$ NMR (298 K, 75 MHz, CD_3OD): δ 179.0 (CO), 150.5 (C_{NCN}), 124.3, 123.4 (CH), 76.6 (CHCOO), 71.3 (=CH cod), 38.4 (NCH_3), 35.0 ($>\text{CH}_2$ cod).

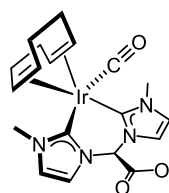


Figure 5. Complex 2.

3.3.2. Synthesis of $[\text{Ir}(\text{CO})_2\{(\text{MeIm})_2\text{CHCOO}\}]$ (3), Figure 6

A solution of $[\text{Ir}(\text{cod})\{(\text{MeIm})_2\text{CHCOO}\}]$ (1) (20.0 mg, 0.038 mmol) in CH_2Cl_2 (5 mL) was stirred for 16 h under carbon monoxide atmosphere to give a clear yellow solution. The concentration of the solution to ca. 1 mL and slow addition of diethyl ether afforded the compound as a yellow solid that was filtered, washed with cold diethyl ether (3×3 mL) and dried in vacuo. Yield: 9.9 mg, 55%. Anal. Calc. for $\text{C}_{12}\text{H}_{11}\text{IrN}_4\text{O}_4$: C, 30.83; H, 2.37; N, 11.99. Found: C, 30.95; H, 2.28; N, 11.89. MS (ESI+, $\text{CH}_2\text{Cl}_2/\text{MeOH}$, m/z): calcd. for $\text{C}_{11}\text{H}_{12}\text{IrN}_4\text{O}_3$ $[\text{M}-\text{CO}+\text{H}]^+$: 441.05, found: 441.32. IR (ATR, cm^{-1}): 2056, 1987 (CO), 1647 (COO). ^1H NMR (298 K, 300 MHz, CD_3OD): δ 7.57 (d, $J = 1.9$, 2H, CH), 7.39 (d, $J = 1.9$, 2H, CH), 6.78 (s, 1H, CHCOO), 3.93 (s, 6H, NCH_3). $^{13}\text{C}\{^1\text{H}\}$ NMR (298 K, 75 MHz, CD_3OD): δ 183.2 (CO), 170.2 (C_{NCN}), 170.0 (COO), 124.2, 124.0 (CH), 76.3 (CHCOO), 36.1 (NCH_3).

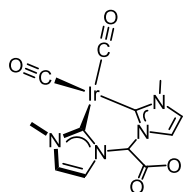


Figure 6. Complex 3.

3.3.3. Synthesis of $[\text{Ir}(\text{cod})\{(\text{MeImCH}_2)_2\text{CHOH}\}]\text{Br}$ (4), Figure 7

NaH (22.0 mg, 60% oil dispersion, 0.550 mmol) and $[\text{Ir}(\mu\text{-Cl})(\text{cod})_2]$ (84.1 mg, 0.125 mmol) were dissolved independently in ethanol (5 mL). The solutions were combined and stirred for 15 min to give a yellow solution which was transferred via cannula to a solution of $[\{(\text{MeImH})\text{CH}_2\}_2\text{CHOH}]\text{Br}_2$ (95.7 mg, 0.250 mmol) in ethanol (5 mL). After stirring for 16 h, the orange solution was brought to dryness under a vacuum, and the orange residue was extracted with dichloromethane (7 mL) and then filtered via cannula. The resulting orange solution was concentrated to ca. 1 mL under reduced pressure. The slow addition of cold diethyl ether resulted in a microcrystalline shiny orange solid, which was washed with diethyl ether (3×3 mL) and dried in vacuo. Yield: 120.1 mg, 80%. Anal. Calc. for $\text{C}_{19}\text{H}_{28}\text{BrIrN}_4\text{O}$: C, 38.00; H, 4.70; N, 9.33. Found: C, 37.99; H, 4.69; N, 9.33. MS (ESI+, $\text{CH}_2\text{Cl}_2/\text{MeOH}$, m/z): calcd. for $\text{C}_{19}\text{H}_{28}\text{IrN}_4\text{O}$ $[\text{M}]^+$: 521.19, found: 521.11. The compound was obtained as two isomers in a 2/1 ratio. *Major isomer*: ^1H NMR (298 K, 400 MHz, CD_2Cl_2): δ 7.37 (d, $J = 1.9$, 2H, CH), 6.80 (d, $J = 1.9$, 2H, CH), 6.25 (s, 1H, OH), 4.70 (br, 2H, NCH_2), 4.47 (br, 2H, NCH_2), 4.47 (s, CHOH), 4.09 (br, 4H, =CH cod), 3.80 (s, 6H, NCH_3), 2.43–2.23 (br, 4H, $>\text{CH}_2$ cod), 2.16–1.95 (br, 4H, $>\text{CH}_2$ cod). $^{13}\text{C}\{^1\text{H}\}$ NMR (298 K, 101 MHz, CD_2Cl_2): δ 178.6 (C_{NCN}), 126.1, 120.9 (CH), 77.2 (=CH cod), 76.0 (=CH cod), 67.1 (CHOH), 55.8 (CH_2), 37.8 (NCH_3), 31.8, 37.8 ($>\text{CH}_2$ cod). *Minor isomer*: ^1H NMR (298 K, 400 MHz, CD_2Cl_2): δ 7.23 (d, $J = 1.8$, 2H, CH), 6.88 (d, $J = 1.9$, 2H, CH), 6.25 (s, 1H, OH), 4.75 (br, 2H, NCH_2), 4.52 (br, 2H, NCH_2), 4.47 (s, CHOH), 4.14 (br, 4H, =CH cod), 3.81 (s, 6H, NCH_3), 2.43–2.23 (br, 4H, $>\text{CH}_2$ cod), 2.16–1.96 (br, 4H, $>\text{CH}_2$ cod). $^{13}\text{C}\{^1\text{H}\}$ NMR (298 K, 101 MHz, CD_2Cl_2): δ 178.3 (C_{NCN}), 124.0, 122.1 (CH), 77.9 (=CH cod), 76.2 (=CH cod), 67.1 (CHOH), 59.1 (CH_2), 37.8 (NCH_3), 31.7, 31.7 ($>\text{CH}_2$ cod).

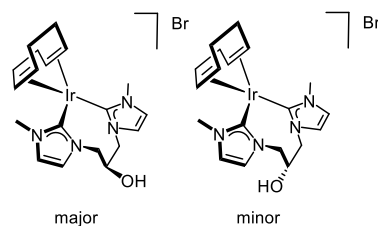


Figure 7. Diastereomers of complex 4.

3.3.4. Synthesis of $[\text{Ir}(\text{CO})_2\{(\text{MeImCH}_2)_2\text{CHOH}\}]\text{Br}$ (5), Figure 8

Carbon monoxide was bubbled through a solution of complex $[\text{Ir}(\text{cod})\{(\text{MeIm}_2\text{CH}_2)_2\text{CHOH}\}]\text{Br}$ (4) (90.0 mg, 0.164 mmol) in CH_2Cl_2 (5 mL) for 10 min to give a pale yellow solution which was concentrated to ca. 1 mL under reduced pressure. The addition of cold diethyl ether (2 mL) afforded a pale-yellow solid, which was filtered, washed with diethyl ether (3×3 mL) and dried in vacuo. Yield: 72.3 mg, 80%. Anal. Calc. for $\text{C}_{13}\text{H}_{16}\text{BrIrN}_4\text{O}_3$: C, 28.47; H, 2.94; N, 10.22. Found: C, 28.39; H, 2.68; N, 10.18. MS (ESI+, $\text{CH}_2\text{Cl}_2/\text{MeOH}$, m/z): calcd. for $\text{C}_{13}\text{H}_{16}\text{IrN}_4\text{O}_3$ $[\text{M}]^+$: 469.08, found: 469.00. IR (ATR, cm^{-1}): 2058, 1985 (CO). The compound was obtained as two isomers in a 4/1 ratio. *Major isomer*: ^1H NMR (298 K, 300 MHz, CD_2Cl_2): δ 7.54 (d, $J = 1.9$, 2H, CH), 6.93 (d, $J = 1.8$, 2H, CH), 6.22 (s, 1H, OH), 4.69–4.50 (br, 4H, CH_2), 4.41 (s, 1H, CHO), 3.79 (s, 3H, NCH_3). $^{13}\text{C}\{^1\text{H}\}$ NMR (298 K, 75 MHz, CD_2Cl_2): δ 182.3 (CO), 169.3 (C_{NCH_3}), 127.6, 122.5 (CH), 65.3 (CHO), 56.4 (CH_2), 38.7 (NCH_3). *Minor isomer*: ^1H NMR (298 K, 300 MHz, CD_2Cl_2): δ 7.46 (d, $J = 1.8$, 2H, CH), 7.02 (d, $J = 1.8$, 2H, CH), 6.22 (s, 1H, OH), 4.69–4.50 (br, 4H, CH_2), 4.41 (s, 1H, CHO), 3.80 (s, 6H, NCH_3). $^{13}\text{C}\{^1\text{H}\}$ NMR (298 K, 75 MHz, CD_2Cl_2): δ 182.3 (CO), 169.3 (C_{NCH_3}), 125.4, 123.8 (CH), 70.5 (CHO), 59.4 (CH_2), 38.7 (NCH_3).

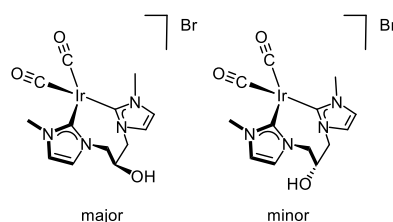


Figure 8. Diastereomers of complex 5.

3.3.5. Synthesis of $[\text{Ir}(\text{cod})\{(\text{MeIm})_2\text{CH}_2\}]\text{I}$ (6), Figure 9

To a suspension of $[\text{Ir}(\mu\text{-Cl})(\text{cod})]_2$ (73.2 mg, 0.11 mmol) in ethanol (5 mL) was slowly added a solution of NaH (13 mg, 0.48 mmol) in ethanol (2 mL), and the mixture was stirred at room temperature for 30 min. Then, the imidazolium salt $[(\text{MeImH})_2\text{CH}_2]\text{I}_2$ (94.2 mg, 0.218 mmol) was added and the suspension was stirred for 24 h. The solvent was pumped off and the residue was extracted with CH_2Cl_2 (2×5 mL). The solution was concentrated under a vacuum to 1 mL, and then diethylether (10 mL) was added to give the compounds as orange-yellow solids that were washed with diethylether (2×5 mL) and dried under vacuum. Yield: 83.2 mg, 63%. Anal. Calc. for $\text{C}_{17}\text{H}_{24}\text{IrN}_4$: C 33.83; H, 4.01; N, 9.28. Found: C, 33.92; H, 4.40; N, 9.01. MS (ESI+, MeOH, m/z): calcd. for $\text{C}_{17}\text{H}_{24}\text{IrN}_4$ $[\text{M}]^+$: 477.17, found: 477.20. ^1H NMR (298 K, 400 MHz, CD_2Cl_2): δ 7.26 (d, $J_{\text{H-H}} = 2.0$, 2H, CH Im), 6.81 (d, $J_{\text{H-H}} = 2.0$, 2H, CH), 6.03 (d, $J_{\text{H-H}} = 11.9$, 1H, NCH_2N), 5.82 (d, $J_{\text{H-H}} = 11.9$, 1H, NCH_2N), 3.82 (m, 4H, $=\text{CH}$ cod), 3.79 (s, 6H, NCH_3), 2.32–2.06 (m, 4H, $>\text{CH}_2$ cod), 2.01–1.80 (m, 4H, $>\text{CH}_2$ cod). $^{13}\text{C}\{^1\text{H}\}$ NMR (298 K, 101 MHz, CD_2Cl_2): δ 172.1 (C_{NCH_3}), 122.2, 119.2 (CH Im), 63.9 ($=\text{CH}$ cod) and (NCH_2N), 39.3 (NCH_3), 33.2 ($>\text{CH}_2$ cod).

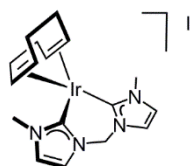


Figure 9. Complex 6.

3.3.6. Synthesis of $[\text{IrCl}(\text{cod})\{\text{MeIm}(\text{CH}_2)_3\text{OH}\}]\text{I}$ (7), Figure 10

A mixture of $[\text{Ir}(\mu\text{-OMe})(\text{cod})]_2$ (189 mg, 0.28 mmol) and $[\text{MeImH}(\text{CH}_2)_3\text{OH}]\text{Cl}$ (100 mg, 0.57 mmol) in THF (10 mL) was stirred overnight at room temperature to give an orange suspension. The solid was removed by filtration, and the resulting orange solution

was evaporated to dryness. Treatment of the yellow residue with pentane rendered a yellowish solid, which was separated by decantation, washed with pentane, and dried in a vacuum. Yield: 233 mg, 86%. Anal. Calcd for $C_{15}H_{24}ClN_2OIr$: C, 37.85; H, 5.08; N, 5.89. Found: C, 37.68; H, 5.03; N, 5.86. MS (MALDI-Tof, DIT matrix, CH_2Cl_2 , m/z): calcd. for $C_{15}H_{25}N_2OIr$ $[M-Cl+H]^+$: 441.59, found: 441.29, Λ_M (acetone): $12 \Omega^{-1} cm^2 mol^{-1}$. 1H NMR (298 K, 300 MHz, $CDCl_3$): δ 6.85, (q, $J = 1.9$, 2H, CH Im), 5.22 (dd, $J = 11.5$, 4.1, 1H, NCH₂), 4.61, 4.54 (m, 2H, =CH cod), 4.01 (dt, $J = 13.8$, 4.1, 1H, NCH₂), 3.94 (s, 3H, MeIm), 3.56, 3.47 (m, 2H, CH₂O), 3.14 (m, 1H, OH), 2.98, 2.90 (m, 2H, =CH cod), 2.22 (m, 4H, >CH₂ cod), 2.11–1.88 (m, 2H, CH₂), 1.80–1.54 (m, 4H, >CH₂ cod). $^{13}C\{^1H\}$ NMR (298 K, 75 MHz, $CDCl_3$): δ 180.2 (NCN), 122.5, 119.3 (CH Im), 85.1, 84.4 (=CH cod), 56.7 (CH₂O), 52.5, 52.2 (=CH cod), 46.1 (NCH₂), 37.6 (MeIm), 34.0, 33.3 (>CH₂ cod), 32.7 (CH₂), 30.0, 29.4 (>CH₂ cod). The molecular structure of 7 has been reported in ref. [48].

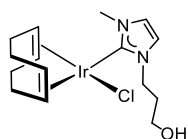


Figure 10. Complex 7.

3.3.7. Synthesis of $[Ir(cod)\{\kappa^2C,O\text{-[MeIm(CH}_2)_3O]\}]$ (8), Figure 11

NaH (5.3 mg, 0.21 mmol) was added to a solution of $[IrCl(cod)\{MeIm(CH_2)_3OH\}]$ (7) (100 mg, 0.21 mmol) in THF (10 mL). The mixture was stirred for 4 h at room temperature. After the elimination of the inorganic salts by filtration, the resulting yellow solution was concentrated until 1 mL. Slow addition of n-hexane (3 mL) afforded an orange solid, which was separated by decantation, washed with n-hexane, and dried in a vacuum. Yield: 76 mg, 82%. Anal. Calcd for $C_{15}H_{23}N_2OIr$: C, 40.99; H, 5.27; N, 6.37. Found: C, 40.86; H, 5.31; N, 6.39. MS (MALDI-Tof, DIT matrix, CH_2Cl_2 , m/z): calcd. for $C_{15}H_{25}N_2OIr$ $[M+2H]^+$: 441.59, found: 441.29; calcd. for $C_{15}H_{27}N_2O_2Ir$ $[M+2H+H_2O]^+$: 459.60, found: 459.21. Λ_M (acetone): $9 \Omega^{-1} cm^2 mol^{-1}$. 1H NMR (298 K, 300 MHz, C_6D_6): δ 6.23, 6.10 (s, 2H, CH Im), 5.24 (m, 1H, NCH₂), 5.11, 5.05 (m, 2H, =CH cod), 3.65 (m, 3H, NCH₂ y CH₂O), 3.50 (s, 3H, MeIm), 2.99 (m, 2H, =CH cod), 2.29 (m, 4H, >CH₂ cod), 1.93, 1.80 (m, 2H, >CH₂), 1.76–1.56 (m, 4H, >CH₂ cod). $^{13}C\{^1H\}$ NMR (298 K, 75 MHz, C_6D_6): δ 180.7 (NCN), 121.9, 119.3 (CH Im), 84.9, 84.2 (=CH cod), 56.9 (CH₂O), 51.6, 51.2 (=CH cod), 46.4 (NCH₂), 37.0 (MeIm), 34.4 (CH₂), 33.6, 33.2, 30.4, 29.6 (>CH₂ cod).

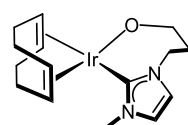


Figure 11. Complex 8.

3.3.8. Synthesis of $[Ir(cod)\{MeIm(CH_2)_3OH\}_2]Cl$ (9), Figure 12

A solution of NaH (24 mg, 1.0 mmol) in ethanol (2 mL) was slowly added to a suspension of $[Ir(\mu-Cl)(cod)]_2$ (101 mg, 0.150 mmol) in ethanol (5 mL), and the mixture was stirred at room temperature for 30 min. Then, the imidazolium salt $[MeImH(CH_2)_3OH]Cl$ (106 mg, 0.6 mmol) was added, and the suspension was stirred for 48 h. The solvent was pumped off, and the residue was extracted with CH_2Cl_2 (2×5 mL). The solution was concentrated under a vacuum to 1 mL, and then diethyl ether (10 mL) was added to give an orange-yellow solid, which was separated by decantation, washed with diethyl ether (2×5 mL) and dried under vacuum. Yield: 140 mg, 72%. HRMS (ESI+, MeOH, m/z): calcd. for $C_{22}H_{36}IrN_4O_2$ $[M]^+$: 580.2507, found: 581.2468. Λ_M (acetone): $54 \Omega^{-1} cm^2 mol^{-1}$. The compound was obtained as two isomers in an 80/20 ratio. Major isomer: 1H NMR (298 K, 300 MHz, CD_2Cl_2): δ : 7.05 (d, $J = 1.0$, 1H, CH Im), 6.94 (d, $J = 1.0$, 1H, CH Im), 5.43 (broad,

1H, OH), 4.75, (ddd, $J = 12.4, 11.7, 5.2$, 1H, NCH₂), 4.25 (ddd, $J = 12.9, 11.7, 5.2$, 1H, NCH₂), 3.91 (m, 2H, =CH cod), 3.89 (s, 3H, MeIm), 3.91, 3.78 (m, 2H, =CH cod), 3.76, 3.64 (m, 2H, CH₂OH), 2.46, 1.86 (m, 2H, NCH₂CH₂), 2.23, 1.95 (m, 4H, >CH₂ cod), 2.04, 1.96 (m, 4H, >CH₂ cod). ¹³C{¹H} NMR (298K, 75 MHz, CD₂Cl₂): δ 177.8 (NCN), 123.1, 121.2 (CH Im), 77.3, 76.1 (=CH cod), 58.8 (CH₂OH), 49.6 (NCH₂), 38.3 (CH₃), 34.7 (NCH₂CH₂), 32.0, 31.6 (>CH₂ cod). *Minor isomer*: ¹H NMR (298 K, 300 MHz, CD₂Cl₂): δ : 7.19 (m, 1H, CH Im), 7.01 (m, 1H, CH Im), 4.41, 4.17 (m, 2H, NCH₂), 4.10, 3.57 (m, 2H, =CH cod), 4.07 (s, 3H, MeIm), 4.10, 3.57 (m, 4H, =CH cod), 2.6–1.8 (m, 4H, >CH₂ cod). ¹³C{¹H} NMR (298K, 75 MHz, CD₂Cl₂): δ 176.6 (NCN), 123.4, 121.8 (CH Im), 78.2, 74.5 (=CH cod), 48.6 (NCH₂), 38.9 (CH₃).

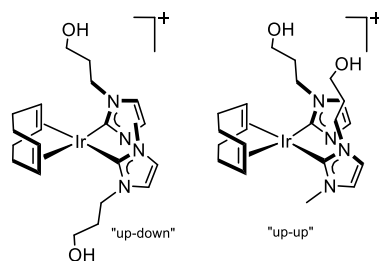


Figure 12. Diastereomers of complex 9.

3.4. General Procedure for the Acceptorless Dehydrogenation of Glycerol

The catalytic reactions were carried out in 25 mL round bottom flasks fitted with a reflux condenser open to the atmosphere. In a typical experiment, the flask was charged under an argon atmosphere with glycerol (1 mL, 13.7 mmol), KOH (312 mg, 5 mmol) and the iridium catalyst and then placed in a thermostatic bath at the desired temperature. The reaction mixture was stirred for the required reaction time and then cooled to room temperature. The resulting suspension was dissolved in 4 mL of MeOH, and then a 0.2 mL aliquot was transferred to a flask. The solvent was removed under vacuum, and the residue was dissolved in D₂O (0.5 mL), and then NaOAc·3H₂O (30 mg, 0.22 mmol) was added as an internal standard. The yield, with respect to the maximum number of mmol of glycerol that can be transformed, is determined by the amount of base (5 mmol), and the selectivity (lactate salt and 1,2-propanediol) was determined by ¹H NMR.

H₂(g) evolution was monitored in a close microreactor equipped with a pressure transducer (Man on the Moon series X102 kit microreactor, www.manonthemoontech.com accessed on 7 November 2022). In a typical experiment, a 43 mL microreactor was charged with glycerol (1 mL, 13.7 mmol) under argon and was isothermal stabilized to 130 °C. Then, KOH (312 mg, 5 mmol) and the iridium catalyst (0.01 mmol) were added. Hydrogen evolution was measured until constant pressure. The amount of H₂(g) (mmol) produced was calculated by using the Ideal Gas Law.

3.5. Crystal Structure Determination

Single crystals of **2**, **4**, and **5** for the X-ray diffraction studies were grown by slow diffusion of diethyl ether into a saturated solution of **2** in methanol or slow diffusion of diethyl ether into a concentrated solution of **4** or **5** in dichloromethane. X-ray diffraction data were collected at 100(2) K on a Bruker SMART APEX CCD diffractometer with graphite-monochromated Mo–K α radiation ($\lambda = 0.71073$ Å) using ω rotations. Intensities were integrated and corrected for absorption effects with SAINT-PLUS [49] and SADABS [50] programs, both included in the APEX2 package. The structures were solved by the Patterson method with SHELXS-97 [51] and refined by full-matrix least-squares on F2 with SHELXL-2014 [52] under WinGX [53]. Pitch and yaw angles have been calculated according to the literature [54]. Despite the fact that the poor quality of the single crystals of **4** and their weak diffraction patterns ($\theta_{\max} \approx 23^\circ$) lead to a structural determination featuring a low accuracy, the quality of the refined model is good enough to confirm the molecular structure proposed

for **4**. On this basis, crystal data and structure refinement are reported in the following, and a brief discussion of the molecular structure of **4** is also provided. CCDC 2206613 (**2**), 2206611 (**4**) and 2206612 (**5**) contain the supplementary crystallographic data for this paper. These data can be obtained free of charge via <http://www.ccdc.cam.ac.uk/conts/retrieving.html>, accessed on 7th November 2022 (or from the CCDC, 12 Union Road, Cambridge CB2 1EZ, UK; Fax: +44 1223 336033; E-mail: deposit@ccdc.cam.ac.uk).

3.5.1. Crystal Data and Structure Refinement for **2**

$C_{19}H_{23}IrN_4O_3 \cdot 2CH_3OH$, 611.70 g·mol⁻¹, orthorhombic, *Pbca*, $a = 13.0008(7)$ Å, $b = 21.0903(12)$ Å, $c = 32.4548(18)$ Å, $V = 8898.8(9)$ Å³, $Z = 16$, $D_{calc} = 1.826$ g·cm⁻³, $\mu = 6.042$ mm⁻¹, $F(000) = 4832$, orange prism, $0.200 \times 0.095 \times 0.065$ mm³, $\theta_{min}/\theta_{max} 1.255/26.372^\circ$, index ranges $-16 \leq h \leq 16$, $-26 \leq k \leq 26$, $-40 \leq l \leq 40$, reflections collected/independent 96,702/9102 [R(int) = 0.0764], $T_{max}/T_{min} 0.5056/0.3386$, data/restraints/parameters 9102/6/564, GooF(F²) 1.197, $R_1 = 0.0399$ [I > 2σ(I)], $wR_2 = 0.0704$ (all data), largest diff. peak/hole 1.291/−1.241 e·Å⁻³. NHC@C1: pitch, θ 0.2°, yaw, ψ 2.3°; NHC@C9: pitch, θ 0.3°; yaw, ψ 3.7°.

3.5.2. Crystal Data and Structure Refinement for **4**

$C_{19}H_{28}IrN_4O_2Br_2 \cdot 3.5CH_2Cl_2$, 1498.37 g·mol⁻¹, monoclinic, *C2/c*, $a = 31.847(2)$ Å, $b = 11.7279(9)$ Å, $c = 30.685(2)$ Å, $\beta = 113.4620(10)^\circ$, $V = 10,513.2(14)$ Å³, $Z = 8$, $D_{calc} = 1.893$ g cm⁻³, $m = 6.977$ mm⁻¹, $F(000) = 5816$, $0.130 \times 0.110 \times 0.090$ mm³, orange prism, $\theta_{min}/\theta_{max} 1.559/23.318^\circ$, index ranges $-35 \leq h \leq 35$, $-13 \leq k \leq 13$, $-34 \leq l \leq 34$, reflections collected/independent 44,589, 7574 [R(int) = 0.0900], $T_{max}/T_{min} 0.8727/0.4738$, data/restraints/parameters 7574/7/579, GooF(F²) 1.124, $R_1 = 0.0566$ [I > 2σ(I)], $wR_2 = 0.1109$ (all data), largest diff. peak/hole 1.574/−1.126 e·Å⁻³. NHC@C1: pitch 6.6°, yaw 2.0°; NHC@C11: pitch 5.1°, yaw 2.4°.

3.5.3. Crystal Data and Structure Refinement for **5**

$C_{13}H_{16}BrIrN_4O_3 \cdot CH_2Cl_2$, 633.33 g·mol⁻¹, Monoclinic, *P2₁/c*, $a = 27.021(9)$ Å, $b = 13.060(4)$ Å, $c = 11.002(4)$ Å, $\beta = 90.569(4)^\circ$, $V = 3882(2)$ Å³, $Z = 8$, $D_{calc} = 2.167$ g·cm³, $\mu = 9.232$ mm⁻¹, $F(000) = 2400$, yellow prism, $0.180 \times 0.108 \times 0.070$ mm³, $\theta_{min}/\theta_{max} 1.507/26.372^\circ$, index ranges $-33 \leq h \leq 33$, $-16 \leq k \leq 16$, $-13 \leq l \leq 13$, reflections collected/independent 43,047/7929 [R(int) = 0.0717], $T_{max}/T_{min} 0.524/0.329$, data/restraints/parameters 7929/0/458, GooF(F²) 1.058, $R_1 = 0.0537$ [I > 2σ(I)], $wR_2 = 0.1213$, largest diff. peak/hole 3.260/−1.684 e·Å⁻³. NHC@C1: pitch 10.2°, yaw 3.2°; NHC@C11: pitch 7.0°, yaw 0.8°.

4. Conclusions

A series of mononuclear iridium(I) catalysts featuring carboxylate and hydroxy bridge-functionalized bis-NHC ligands and a cationic unbridged bis-NHC iridium(I) complex bearing 3-hydroxypropyl functionalized NHC ligands have been synthesized and characterized. These catalysts have been shown to be highly active for the selective oxidation of glycerol to lactic acid via acceptorless dehydrogenation of neat glycerol in the presence of KOH as a base. The acetate and hydroxy functions in bis-NHC iridium(I) catalysts increase their solubility in the reaction medium, which results in a significant activity improvement compared to the related iridium(I) catalysts featuring a bridge-unfunctionalized bis-NHC ligand. The hydroxy-functionalized bis-NHC catalysts were found to be much more active than the carboxylate-functionalized ones, and the unbridged bis-NHC iridium(I) catalyst with hydroxyalkyl functionalized NHC ligands. Interestingly, the related neutral chlorido-complex featuring only a hydroxyalkyl-functionalized NHC ligand exhibited a notable catalytic activity. In general, carbonyl complexes are more active than the related diene complexes, with [Ir(CO)₂{(MeImCH₂)₂CHOH}]Br as the most active catalyst affording TONs to LA up to 15,000 at very low catalyst loadings. The high catalytic activity of bridge-functionalized bis-NHC iridium(I) complexes highlights their potential for the development of practical technologies for the transformation of glycerol into value-added chemicals.

Supplementary Materials: The following supporting information can be downloaded at: <https://www.mdpi.com/article/10.3390/molecules27227666/s1>, selected NMR, IR and HRMS spectra of iridium(I) compounds and ¹H NMR analysis representative of a catalysis test in the standard reaction conditions.

Author Contributions: The manuscript was written through the contributions of all authors. Conceptualization, M.V.J. and J.J.P.-T.; X-ray analysis, V.P.; Funding acquisition, M.V.J. and J.J.P.-T.; Investigation, A.I.O.-A., R.P.-O. and J.M.-S.; Methodology, M.V.J.; Validation, A.I.O.-A., R.P.-O. and J.M.-S.; Writing—original draft, M.V.J.; Writing—review & editing, M.V.J. and J.J.P.-T. All authors have read and agreed to the published version of the manuscript.

Funding: This research was funded by the Spanish Ministerio de Ciencia e Innovación MCIN/AEI/10.13039/501100011033, under the Project PID2019-103965GB-I00, and the Departamento de Ciencia, Universidad y Sociedad del Conocimiento del Gobierno de Aragón (group E42_20R).

Institutional Review Board Statement: Not available.

Informed Consent Statement: Not available.

Data Availability Statement: Not available.

Acknowledgments: J.M.-S. acknowledges the Gobierno de Aragón for a Pre-Doctoral fellowship.

Conflicts of Interest: The authors declare that they have no conflict of interest.

References

1. Takkellapati, S.; Li, T.; González, M.A. An Overview of Biorefinery Derived Platform Chemicals from a Cellulose and Hemicellulose Biorefinery. *Clean Technol. Environ. Policy* **2018**, *20*, 1615–1630. [[CrossRef](#)]
2. Chilakamarri, C.R.; Sakinah, A.M.M.; Zularisam, A.W.; Pandey, A. Glycerol waste to value added products and its potential applications. *Syst. Microbiol. Biomanuf.* **2021**, *1*, 378–396. [[CrossRef](#)]
3. Dusselier, M.; Van Wouwe, P.; Dewaele, A.; Makshina, E.; Sels, B.F. Lactic acid as a platform chemical in the biobased economy: The role of chemocatalysis. *Energy Environ. Sci.* **2014**, *6*, 1415–1442. [[CrossRef](#)]
4. Morales, M.; Dapsens, P.Y.; Giovinazzo, I.; Witte, J.; Mondelli, C.; Papadokonstantakis, S.; Hungerbühler, K.; Perez-Ramirez, J. Environmental and economic assessment of lactic acid production from glycerol using cascade bio- and chemocatalysis. *Energy Environ. Sci.* **2015**, *8*, 558–567. [[CrossRef](#)]
5. Wang, K.; Yang, Z.; Ma, Y.; Zhao, W.; Sun, J.; Lu, T.; He, H. Recent advances in the utilization of glycerol for the production of lactic acid by catalysis. *Biofuels Bioprod. Bioref.* **2022**, *16*, 1428–1454. [[CrossRef](#)]
6. Montassier, C.; Menezo, J.C.; Hoang, L.C.; Renaud, C.; Barbier, J. Aqueous polyol conversions on ruthenium and on sulfur-modified ruthenium. *J. Mol. Catal.* **1991**, *70*, 99–110. [[CrossRef](#)]
7. Maris, E.P.; Davis, R.J. Hydrogenolysis of glycerol over carbon-supported Ru and Pt catalysts. *J. Catal.* **2007**, *249*, 328–337. [[CrossRef](#)]
8. Roy, D.; Subramaniam, B.; Chaudhari, R.V. Kinetic Modeling of Aqueous-Phase Glycerol Hydrogenolysis in a Batch Slurry Reactor. *ACS Catal.* **2011**, *1*, 548–551. [[CrossRef](#)]
9. Akbulut, D.; Ozkar, S. A review of the catalytic conversion of glycerol to lactic acid in the presence of aqueous base. *RSC Adv.* **2022**, *12*, 18864–18883. [[CrossRef](#)]
10. Kumar, A.; Gao, G. Homogeneous (De)hydrogenative Catalysis for Circular Chemistry—Using Waste as a Resource. *ChemCatChem* **2021**, *13*, 1105–1134. [[CrossRef](#)]
11. Lu, Z.; Cherepakhin, V.; Demianets, I.; Lauridsen, P.J.; Williams, T.J. Iridium-based hydride transfer catalysts: From hydrogen storage to fine chemicals. *Chem. Commun.* **2018**, *54*, 7711–7724. [[CrossRef](#)] [[PubMed](#)]
12. Bielinski, E.A.; Lagaditis, P.O.; Zhang, Y.; Mercado, B.Q.; Würtele, C.; Bernskoetter, W.H.; Hazari, N.; Schneider, S. Lewis Acid-Assisted Formic Acid Dehydrogenation Using a Pincer-Supported Iron Catalyst. *J. Am. Chem. Soc.* **2014**, *136*, 10234–10237. [[CrossRef](#)]
13. Chakraborty, S.; Lagaditis, P.O.; Förster, M.; Bielinski, E.A.; Hazari, N.; Holthausen, M.C.; Jones, W.D.; Schneider, S. Well-Defined Iron Catalysts for the Acceptorless Reversible Dehydrogenation-Hydrogenation of Alcohols and Ketones. *ACS Catal.* **2014**, *4*, 3994–4003. [[CrossRef](#)]
14. Bielinski, E.A.; Förster, M.; Zhang, Y.; Bernskoetter, W.H.; Hazari, N.; Holthausen, M.C. Base-Free Methanol Dehydrogenation Using a Pincer-Supported Iron Compound and Lewis Acid Co-catalyst. *ACS Catal.* **2015**, *5*, 2404–2415. [[CrossRef](#)]
15. Alberico, E.; Sponholz, P.; Cordes, C.; Nielsen, M.; Drexler, H.J.; Baumann, W.; Junge, H.; Beller, M. Selective Hydrogen Production from Methanol with a Defined Iron Pincer Catalyst under Mild Conditions. *Angew. Chem. Int. Ed.* **2013**, *52*, 14162–14166. [[CrossRef](#)]
16. Chakraborty, S.; Brennessel, W.W.; Jones, W.D.A. Molecular Iron Catalyst for the Acceptorless Dehydrogenation and Hydrogenation of N-Heterocycles. *J. Am. Chem. Soc.* **2014**, *136*, 8564–8567. [[CrossRef](#)]

17. Sharninghausen, L.S.; Mercado, B.Q.; Crabtree, R.H.; Hazari, N. Selective conversion of glycerol to lactic acid with iron pincer precatalysts. *Chem. Commun.* **2015**, *51*, 16201–16204. [[CrossRef](#)]
18. Li, Y.; Nielsen, M.; Li, B.; Dixneuf, P.H.; Junge, H.; Beller, M. Ruthenium-catalyzed hydrogen generation from glycerol and selective synthesis of lactic acid. *Green Chem.* **2015**, *17*, 193198. [[CrossRef](#)]
19. Kirchhecker, S.; Spiegelberg, B.; de Vries, J.G. Homogenous Iridium Catalysts for Biomass Conversion. In *Iridium Catalysts for Organic Reactions*; Oro, L.A., Claver, C., Eds.; Springer: Berlin/Heidelberg, Germany, 2020; Volume 69, pp. 341–395.
20. Sharninghausen, L.S.; Campos, J.; Manas, M.G.; Crabtree, R.H. Efficient selective and atom economic catalytic conversion of glycerol to lactic acid. *Nat. Commun.* **2014**, *5*, 5084. [[CrossRef](#)]
21. Lu, Z.; Demianets, I.; Hamze, R.; Terrile, N.J.; Williams, T.J. A Prolific Catalyst for Selective Conversion of Neat Glycerol to Lactic Acid. *ACS Catal.* **2016**, *6*, 2014–2017. [[CrossRef](#)]
22. Finn, M.; Ridenour, J.A.; Heltzel, J.; Cahill, C.; Voutchkova-Kostal, A. Next-Generation Water-Soluble Homogeneous Catalysts for Conversion of Glycerol to Lactic Acid. *Organometallics* **2018**, *37*, 1400–1409. [[CrossRef](#)]
23. Puerta-Oteo, R.; Ojeda-Amador, A.I.; Jiménez, M.V.; Pérez-Torrente, J.J. Catalytic applications of zwitterionic transition metal compounds. *Dalton Trans.* **2022**, *51*, 817–830. [[CrossRef](#)] [[PubMed](#)]
24. Poyatos, M.; Mata, J.A.; Peris, E. Complexes with Poly(N-heterocyclic carbene) Ligands: Structural Features and Catalytic Applications. *Chem. Rev.* **2009**, *109*, 3677–3707. [[CrossRef](#)]
25. Cheong, Y.-J.; Sung, K.; Kim, J.-A.; Kim, Y.K.; Jang, H.-Y. Highly Efficient Iridium-Catalyzed Production of Hydrogen and Lactate from Glycerol: Rapid Hydrogen Evolution by Bimetallic Iridium Catalysts. *Eur. J. Inorg. Chem.* **2020**, 4064–4068. [[CrossRef](#)]
26. Sun, Z.; Liu, Y.; Chen, J.; Huang, C.; Tu, T. Robust Iridium Coordination Polymers: Highly Selective, Efficient, and Recyclable Catalysts for Oxidative Conversion of Glycerol to Potassium Lactate with Dihydrogen Liberation. *ACS Catal.* **2015**, *5*, 6573–6578. [[CrossRef](#)]
27. Puerta-Oteo, R.; Jiménez, M.V.; Lahoz, F.J.; Modrego, F.J.; Passarelli, V.; Pérez-Torrente, J.J. Zwitterionic rhodium and iridium complexes based on a carboxylate bridge-functionalized bis-N-heterocyclic carbene ligand: Synthesis, structure, dynamic behavior, and reactivity. *Inorg. Chem.* **2018**, *57*, 5526–5543. [[CrossRef](#)]
28. Puerta-Oteo, R.; Munarriz, J.; Polo, V.; Jiménez, M.V.; Pérez-Torrente, J.J. Carboxylate-Assisted β -(Z) Stereoselective Hydrosilylation of Terminal Alkynes Catalyzed by a Zwitterionic Bis-NHC Rhodium(III) Complex. *ACS Catal.* **2020**, *10*, 7367–7380. [[CrossRef](#)]
29. Ojeda-Amador, A.I.; Munarriz, J.; Alamán-Valtierra, P.; Polo, V.; Puerta-Oteo, R.; Jiménez, M.V.; Fernández-Alvarez, F.J.; Pérez-Torrente, J.J. Mechanistic Insights on the Functionalization of CO₂ with Amines and Hydrosilanes Catalyzed by a Zwitterionic Iridium Carboxylate-Functionalized Bis-NHC Catalyst. *ChemCatChem* **2019**, *11*, 5524–5535. [[CrossRef](#)]
30. Puerta-Oteo, R.; Hölscher, M.; Jiménez, M.V.; Leitner, W.; Passarelli, V.; Pérez-Torrente, J.J. Experimental and Theoretical Mechanistic Investigation on the Catalytic CO₂ Hydrogenation to Formate by a Carboxylate-Functionalized Bis(N-heterocyclic carbene) Zwitterionic Iridium(I) Compound. *Organometallics* **2018**, *37*, 684–696. [[CrossRef](#)]
31. Puerta-Oteo, R.; Jiménez, M.V.; Pérez-Torrente, J.J. Molecular water oxidation catalysis by zwitterionic carboxylate bridge-functionalized bis-NHC iridium complexes. *Catal. Sci. Technol.* **2018**, *9*, 1437–1450. [[CrossRef](#)]
32. Desai, S.P.; Mondal, M.; Choudhury, J. Chelating Bis-N-heterocyclic Carbene–Palladium(II) Complexes for Oxidative Arene C–H Functionalization. *Organometallics* **2015**, *34*, 2731–2736. [[CrossRef](#)]
33. Zhong, R.; Pöthig, A.; Mayer, D.C.; Jandl, C.; Altmann, P.J.; Herrmann, W.A.; Kühn, F.E. Spectroscopic and Structural Properties of Bridge-Functionalized Dinuclear Coinage-Metal (Cu, Ag, and Au) NHC Complexes: A Comparative Study. *Organometallics* **2015**, *34*, 2573–2579. [[CrossRef](#)]
34. Zhong, R.; Pöthig, A.; Haslinger, S.; Hofmann, B.; Raudaschl-Sieber, G.; Herdtweck, E.; Herrmann, W.A.; Kühn, F.E. Toward Tunable Immobilized Molecular Catalysts: Functionalizing the Methylene Bridge of Bis(N-heterocyclic carbene) Ligands. *ChemPlusChem* **2014**, *79*, 1294–1303. [[CrossRef](#)]
35. Quezada, C.; Garrison, J.C.; Tessier, C.A.; Youngs, W.J. Synthesis and structural characterization of two bis(imidazol-2-ylidene) complexes of Pt(II). *J. Organomet. Chem.* **2003**, *671*, 183–186. [[CrossRef](#)]
36. Bekhouche, M.; Blum, L.J.; Doumèche, B. Ionic liquid-inspired cations covalently bound to FDH improve its stability and activity in IL. *ChemCatChem* **2011**, *3*, 875–882. [[CrossRef](#)]
37. Blanco, M.; Alvarez, P.; Blanco, C.; Jiménez, M.V.; Fernández-Tornos, J.; Pérez-Torrente, J.J.; Oro, L.A.; Menendez, R. Enhanced hydrogen-transfer catalytic activity of iridium N-heterocyclic carbenes by covalent attachment on carbon nanotubes. *ACS Catalysis* **2013**, *3*, 1307–1317. [[CrossRef](#)]
38. Couzijn, E.P.A.; Slootweg, J.C.; Ehlers, A.W.; Lammertsma, K. Stereomutation of Pentavalent Compounds: Validating the Berry Pseudorotation, Redressing Ugi’s Turnstile Rotation, and Revealing the Two- and Three-Arm Turnstiles. *J. Am. Chem. Soc.* **2010**, *132*, 18127–18140. [[CrossRef](#)]
39. Straubinger, C.S.; Jokić, N.B.; Högerl, M.P.; Herdtweck, E.; Herrmann, W.A.; Kühn, F.E. Bridge functionalized bis-N-heterocyclic carbene rhodium(I) complexes and their application in catalytic hydrosilylation. *J. Organomet. Chem.* **2011**, *696*, 687–692. [[CrossRef](#)]
40. Jiménez, M.V.; Fernández-Tornos, J.; Pérez-Torrente, J.J.; Modrego, F.J.; García-Orduña, P.; Oro, L.A. Mechanistic Insights into Transfer Hydrogenation Catalysis by [Ir(cod)(NHC)₂]⁺ Complexes with Functionalized N-Heterocyclic Carbene Ligands. *Organometallics* **2015**, *34*, 926–940. [[CrossRef](#)]

41. Brookhart, M.; Green, M.L.H.; Parkin, G. Agostic interactions in transition metal compounds. *Proc. Natl. Acad. Sci. USA* **2007**, *104*, 6908–6914. [[CrossRef](#)] [[PubMed](#)]
42. Frey, G.D.; Rentzsch, C.F.; von Preysing, D.; Scherg, T.; Mühlhofer, M.; Herdtweck, E.; Herrmann, W.A. Rhodium and iridium complexes of N-heterocyclic carbenes: Structural investigations and their catalytic properties in the borylation reaction. *J. Organomet. Chem.* **2006**, *691*, 5725–5738. [[CrossRef](#)]
43. Rentzsch, C.F.; Tosh, E.; Herrmann, W.A.; Kühn, F.E. Iridium complexes of N-heterocyclic carbenes in C–H borylation using energy efficient microwave technology: Influence of structure, ligand donor strength and counter ion on catalytic activity. *Green Chem.* **2009**, *11*, 1610–1617. [[CrossRef](#)]
44. Jiménez, M.V.; Pérez-Torrente, J.J.; Bartolomé, M.I.; Gierz, V.; Lahoz, F.J.; Oro, L.A. Rhodium (I) complexes with hemilabile N-heterocyclic carbenes: Efficient alkyne hydrosilylation catalysts. *Organometallics* **2008**, *27*, 224–234. [[CrossRef](#)]
45. Herde, J.L.; Lambert, J.C.; Senoff, C.V.; Cushing, M.A. Cyclooctene and 1,5-Cyclooctadiene Complexes of Iridium(I). *Inorg. Synth.* **2007**, *15*, 18–20.
46. Usón, R.; Oro, L.A.; Cabeza, J.A. Dinuclear methoxy, cyclooctadiene, and barrelene complexes of rhodium(I) and iridium(I). *Inorg. Synth.* **1985**, *23*, 126–127.
47. Ulmer, L.; Mattay, J.; Torres-García, H.G.; Luftmann, H. The Use of 2-[(2E)-3-(4-Tert-Butylphenyl)-2-Methylprop-2-Enylidene]Malononitrile as a Matrix for Matrix-Assisted Laser Desorption/Ionization Mass Spectrometry. *Eur. J. Mass Spectrom.* **2000**, *6*, 49–52. [[CrossRef](#)]
48. Blanco, M.; Álvarez, P.; Blanco, C.; Jiménez, M.V.; Fernández-Tornos, J.; Pérez-Torrente, J.J.; Blasco, J.; Subías, G.; Cuartero, V.; Oro, L.A.; et al. Effect of structural differences of carbon nanotubes and graphene based iridium-NHC materials on the hydrogen transfer catalytic activity. *Carbon* **2016**, *96*, 66–74. [[CrossRef](#)]
49. SAINT+: *Area-Detector Integration Software*, version 6.01; Bruker AXS: Madison, WI, USA, 2001.
50. Sheldrick, G.M. *SADABS Program*; University of Göttingen: Göttingen, Germany, 1999.
51. Sheldrick, G.M. *SHELXS 97, Program for the Solution of Crystal Structure*; University of Göttingen: Göttingen, Germany, 1997.
52. Sheldrick, G.M. Crystal structure refinement with SHELXL. *Acta Crystallogr. Sect. C Struct. Chem.* **2015**, *71*, 3–8. [[CrossRef](#)]
53. Farrugia, L.J. WinGX and ORTEP for Windows: An update. *J. Appl. Crystallogr.* **2012**, *45*, 849–854. [[CrossRef](#)]
54. Azpíroz, R.; Rubio-Pérez, L.; Di Giuseppe, A.; Passarelli, V.; Lahoz, F.J.; Castarlenas, R.; Pérez-Torrente, J.J.; Oro, L.A. Rhodium(I)-N-Heterocyclic Carbene Catalyst for Selective Coupling of N-Vinylpyrazoles with Alkynes via C–H Activation. *ACS Catal.* **2014**, *4*, 4244–4253. [[CrossRef](#)]